Brain, Behavior, and Immunity 120 (2024) 121–140

Contents lists available at ScienceDirect

Brain Behavior and Immunity

journal homepage: www.elsevier.com/locate/ybrbi

Opposing effects of the purinergic P2X7 receptor on seizures in neurons and microglia in male mice

Mariana Alves [a], Beatriz Gil [a], Javier Villegas-Salmerón [a,b,c], Valentina Salari [d], Ricardo Martins-Ferreira [e,f,g,h], Marina Arribas Blázquez [i], Aida Menéndez Méndez [a,j], Rogerio Da Rosa Gerbatin [a,b], Jonathon Smith [a,b], Laura de Diego-Garcia [a,k], Giorgia Conte [a], Juan Sierra-Marquez [l,m,s,t], Paula Merino Serrais [m], Meghma Mitra [a], Ana Fernandez Martin [a], Yitao Wang [a,n], Jaideep Kesavan [a,b], Ciara Melia [a,u], Alberto Parras [a], Edward Beamer [a,o], Béla Zimmer [l], Mona Heiland [a,b], Brenton Cavanagh [p], Rafael Parcianello Cipolat [a,b], James Morgan [a,q], Xinchen Teng [n], Jochen H.M. Prehn [a,b], Paolo F. Fabene [d,v,w], Giuseppe Bertini [d], Antonio R. Artalejo [i], Esteban Ballestar [e,r], Annette Nicke [l], Luis A. Olivos-Oré [i], Niamh M.C. Connolly [a,b], David C. Henshall [a,b], Tobias Engel [a,b,*]

[a] Department of Physiology & Medical Physics, RCSI University of Medicine & Health Sciences, Dublin D02 YN77, Ireland
[b] FutureNeuro, SFI Research Centre for Chronic and Rare Neurological Diseases, RCSI University of Medicine and Health Sciences, Dublin D02 YN77, Ireland
[c] The SFI Centre for Research Training in Genomics Data Science, RCSI University of Medicine & Health Sciences, Dublin D02 YN77, Ireland
[d] Department of Neurosciences, Biomedicine and Movement Sciences, School of Medicine, University of Verona, 37134 Verona, Italy
[e] Epigenetics and Immune Disease Group, Josep Carreras Research Institute (IJC), 08916 Badalona, Barcelona, Spain
[f] Immunogenetics Laboratory, Molecular Pathology and Immunology, Instituto de Ciências Biomédicas Abel Salazar – Universidade do Porto (ICBAS-UP), Rua Jorge Viterbo Ferreira, 228, 4050-313 Porto, Portugal
[g] Autoimmunity and Neuroscience Group, UMIB - Unit for Multidisciplinary Research in Biomedicine, ICBAS - School of Medicine and Biomedical Sciences, University of Porto, Porto, Portugal
[h] ITR - Laboratory for Integrative and Translational Research in Population Health, Porto, Portugal
[i] Department of Pharmacology and Toxicology, Veterinary Faculty, Universidad Complutense de Madrid, Avda. Puerta de Hierro s/n, 28040 Madrid, Spain
[j] Department of Medicine, Faculty of Biomedical and Health Sciences, Universidad Europea de Madrid, 28670, Villaviciosa de Odon, Spain
[k] Ocupharm Research Group, Faculty of Optics and Optometry, Complutense University of Madrid, Avda. Arcos de Jalon, 118 (28037), Madrid, Spain
[l] Walther Straub Institute of Pharmacology and Toxicology, Faculty of Medicine, Ludwig-Maximilians-Universität München, Munich, Germany
[m] Laboratorio Cajal de Circuitos Corticales (CTB), Centro de Tecnología Biomédica, Universidad Politécnica de Madrid, Campus Montegancedo S/N, Pozuelo de Alarcon, 28223 Madrid, Spain
[n] College of Pharmaceutical Sciences, Soochow University, Suzhou, Jiangsu 215123, China
[o] School of Science and Technology, Nottingham Trent University, Nottingham, UK
[p] Cellular and Molecular Imaging Core, Royal College of Surgeons in Ireland, 123 St. Stephen's Green, Dublin 2, Ireland
[q] Division of Developmental Biology and Medicine, School of Medical Sciences, Faculty of Biology, Medicine and Health, University of Manchester, M13 9PL, UK
[r] Epigenetics in Inflammatory and Metabolic Diseases Laboratory, Health Science Center (HSC), East China Normal University (ECNU), Shanghai 200241, China
[s] Instituto Cajal, Consejo Superior de Investigaciones Científicas (CSIC), Madrid 28002, Spain
[t] Centro de Investigación Biomédica en Red de Enfermedades Neurodegenerativas, Instituto de Salud Carlos III, Madrid 28031, Spain
[u] VivoArchitect, Route de la Corniche 5, 1066 Epalinges, Vaud, Switzerland
[v] Section of Anatomy and Histology, Department of Neurosciences, Biomedicine, and Movement Science, Faculty of Medicine, University of Verona, Verona, Italy
[w] Section of Innovation Biomedicine, Department of Engineering for Innovation Medicine, Faculty of Medicine, University of Verona, Verona, Italy

ARTICLE INFO

Keywords:
P2X7 receptor
Status epilepticus
Epilepsy
Cell type-specific function

ABSTRACT

Background: The purinergic ATP-gated P2X7 receptor (P2X7R) is increasingly recognized to contribute to pathological neuroinflammation and brain hyperexcitability. P2X7R expression has been shown to be increased in the brain, including both microglia and neurons, in experimental models of epilepsy and patients. To date, the cell type-specific downstream effects of P2X7Rs during seizures remain, however, incompletely understood.

* Corresponding author.
E-mail address: tengel@rcsi.ie (T. Engel).

https://doi.org/10.1016/j.bbi.2024.05.023
Received 23 December 2023; Received in revised form 28 April 2024; Accepted 19 May 2024
Available online 20 May 2024
0889-1591/© 2024 The Author(s). Published by Elsevier Inc. This is an open access article under the CC BY license (http://creativecommons.org/licenses/by/4.0/).

GABAergic interneurons
Microglia

Methods: Effects of P2X7R signaling on seizures and epilepsy were analyzed in induced seizure models using male mice including the kainic acid model of status epilepticus and pentylenetetrazole model and in male and female mice in a genetic model of Dravet syndrome. RNA sequencing was used to analyze P2X7R downstream signaling during seizures. To investigate the cell type-specific role of the P2X7R during seizures and epilepsy, we generated mice lacking exon 2 of the *P2rx7* gene in either microglia (*P2rx7*:*Cx3cr1*-Cre) or neurons (*P2rx7*:*Thy-1*-Cre). To investigate the protective potential of overexpressing P2X7R in GABAergic interneurons, P2X7Rs were overexpressed using adeno-associated virus transduction under the mDlx promoter.
Results: RNA sequencing of hippocampal tissue from wild-type and P2X7R knock-out mice identified both glial and neuronal genes, in particular genes involved in GABAergic signaling, under the control of the P2X7R following seizures. Mice with deleted *P2rx7* in microglia displayed less severe acute seizures and developed a milder form of epilepsy, and microglia displayed an anti-inflammatory molecular profile. In contrast, mice lacking *P2rx7* in neurons showed a more severe seizure phenotype when compared to epileptic wild-type mice. Analysis of single-cell expression data revealed that human *P2RX7* expression is elevated in the hippocampus of patients with temporal lobe epilepsy in excitatory and inhibitory neurons. Functional studies determined that GABAergic interneurons display increased responses to P2X7R activation in experimental epilepsy. Finally, we show that viral transduction of P2X7R in GABAergic interneurons protects against evoked and spontaneous seizures in experimental temporal lobe epilepsy and in mice lacking *Scn1a*, a model of Dravet syndrome.
Conclusions: Our results suggest a dual and opposing action of P2X7R in epilepsy and suggest P2X7R overexpression in GABAergic interneurons as a novel therapeutic strategy for acquired and, possibly, genetic forms of epilepsy.

1. Introduction

The purinergic P2X7 receptor (P2X7R) has been postulated as a treatment target for numerous diseases of the central nervous system (CNS) including epilepsy (Andrejew, 2020; Sperlagh and Illes, 2014), where it contributes to neuroinflammation and the generation of hyperexcitable neuronal networks (Beamer, 2021; Engel et al., 2021). The P2X7R belongs to the ATP-gated ionotropic P2XR family and forms a channel for the non-selective passage of cations including K^+, Na^+ and Ca^{2+} (Jimenez-Mateos, 2019; Kopp, 2019). The P2X7R has unique structural and functional characteristics which differentiate it from the other P2XRs. This includes an approximately 200 amino acid longer C-terminus, the ability to form a pore that allows the passage of molecules up to 900 Da, and slow desensitization dynamics (Jimenez-Mateos, 2019; Kopp, 2019). Most notably, the P2X7R has a lower affinity for ATP when compared to the other P2XRs, suggesting P2X7R activation occurs mainly within the pathological focus of high extracellular ATP concentrations (Surprenant, 1996). While there is widespread consent for its expression on glial cells including microglia and oligodendrocytes, whether P2X7Rs are expressed and functional on neurons remains a matter of debate (Miras-Portugal, 2017; Illes et al., 2017).

Due to its prominent expression and function on inflammatory cells, the P2X7R has been suggested as a gatekeeper of inflammation contributing to microglia activation and the release of pro-inflammatory mediators (*e.g.*, Interleukin-1β (IL-1β)) (Monif, 2009). Other effects of P2X7R activation have, however, also been reported, including promotion of aberrant synaptic plasticity and neurogenesis, changes in blood–brain barrier (BBB) permeability, T cell activation (Rissiek, 2015), and cell death (Sperlagh and Illes, 2014).

P2X7R expression has consistently been found to be increased in the brains of epilepsy models and patients (Dona, 2009; Morgan, 2020). While several studies have reported anticonvulsive effects when blocking or deleting the P2X7R during status epilepticus (SE) (Jimenez-Pacheco, 2013; Jimenez-Pacheco, 2016; Nieoczym et al., 2017; Huang, 2017), others have reported either no effect (Fischer, 2016; Dogan, 2020) or, in contrast, a pro-convulsant effect (Kim and Kang, 2011; Rozmer, 2017). Of note, a more recent study has shown increased P2X7R function on microglia, leading to a diminished response to anticonvulsants during SE (Beamer, 2022). More consistent data has been observed during epilepsy with P2X7R antagonism reducing seizure severity (Amhaoul, 2016) and frequency (Jimenez-Pacheco, 2016; Mamad, 2023). Regarding its cell type-specific expression and function, whereas a glial and neuronal localisation has been detected using immunohistochemical-based methods in experimental models of epilepsy (Dona, 2009; Morgan, 2020; Jimenez-Pacheco, 2016; Beamer, 2022; Deuchars, 2001; Armstrong, 2002; Engel, 2012), it is uncertain what are their specific roles during seizures and epilepsy, and whether similar expression patterns are observed in human temporal lobe epilepsy (TLE).

Here, we sought to tease apart the actions of the P2X7R in these two cell populations in models of experimental epilepsy. First, mRNA sequencing of hippocampal brain tissue using wild-type (wt) and P2X7R knockout (KO) mice identified both glial and neuronal genes to be under the control of the P2X7R following SE. We then used the conditional Cre-LoxP system to delete the P2X7R in either microglia or neurons. Using mouse models of SE and acute, evoked seizures, our data indicate that the lack of P2X7R expression in neurons has a pro-seizure effect whereas the absence of the receptor in microglia ameliorated seizure severity. We further demonstrate that enhancing expression of P2X7Rs in gamma-aminobutyric acid (GABA)ergic interneurons in mice protects against seizures in models of TLE and Dravet syndrome, a rare epilepsy caused by impaired function of inhibitory interneurons (Bender, 2012). Our findings, therefore, expand on the role of the P2X7R in contributing to microglia-driven pro-inflammatory signaling during seizures, and identified a new anti-convulsive function of the P2X7R on GABAergic inhibitory neurons, suggesting precision-therapy-based approaches may be needed to fully exploit the actions of P2X7Rs for epilepsy and other brain diseases that feature altered brain excitability and neuroinflammation.

2. Material and methods

2.1. Study approval

All animal experiments were performed in accordance with the principles of the European Communities Council Directive (2010/63/EU). Procedures were reviewed and approved by the Research Ethics Committee of the Royal College of Surgeons in Ireland (RCSI) (REC 1322) and Health Products Regulatory Authority (HPRA) (AE19127/P038; AE19127/P013). All animals were treated according to European standards/regulations for animal experiments and all efforts were made to minimize animal suffering and reduce the numbers of animals under experiments.

2.2. Animals

This study included 8–10 weeks old male C57/Bl6 OlaHsd mice, P2X7R knock-out (KO) (*P2rx7*$^{-/-}$) mice (6NTac;B6N-P2rx7tm1d

(EUCOMM)Wtsi/Ieg) which lack exon 2 of the *P2rx7* gene, tamoxifen-inducible Cre lines B6.129P2(Cg)-Cx3cr1tm2.1(cre/ERT2)Litt/WganJ (*Cx3cr*) (JAX stock #021160) and Tg(Thy1-cre/ERT2,-EYFP)HGfng/PyngJ (*Thy-1*) (JAX stock #012708) crossed to mice where the murine exon 2 of the *P2rx7* gene is flanked with loxP sites ($P2rx7^{fl/fl}$) generated by the European Conditional Mouse Mutagenesis (EUCOMM) Program [P2rx7tm1a(EUCOMM)Wtsi] to obtain conditional mice with a *P2rx7* deletion in microglia ($P2rx7^{-/-}$-M) and neurons ($P2rx7^{-/-}$-N). F1.*Scn1a* $(+/-)^{tm1Kea}$ mice (males and females) were generated by crossing *Scn1a* $(+/-)^{tm1Kea}$ male on the 129S6/SvEvTac background (Jackson Laboratory, USA) with inbred female mice C57BL/6JOlaHsd (Envigo, UK) (Miller, 2014). All animals were housed in a controlled biomedical facility using Tecniplast conventional cages (Ref. 1284L EUROSTANDARD TYPE II L) and Lignocel BK8/15–25, premium hygienic animal bedding (D0764P00Z) with 2–5 mice per cage on a 12-hour light/dark cycle at 22 ± 1 °C and humidity of 40–60 % with food and water provided *ad libitum*. For each cage, enrichment was provided in the form of nesting material (irradiated Bed-r'Nest Brown, Datesand, Item code CS1BEB), PVC tubes and red polycarbonate mouse houses. All *in vivo* studies were carried out during the light phase of the cycle.

2.3. Seizure models

For our study, we used different seizure models to test the effects of P2X7R modulation on the seizure threshold. This included its effects on (i) evoked seizures, induced via an intraperitoneal (i.p.) injection of Pentylenetetrazol (PTZ), (ii) status epilepticus (SE), defined as prolonged damaging seizure activity induced via the administration of kainic acid (KA) either i.p. or into the basolateral amygdala, and (iii) epileptic seizures, recurrent unprovoked seizures occurring during epilepsy following intra-amygdala KA (IAKA)-induced SE.

Briefly, SE was induced in mice via an IAKA or via i.p. KA (Alves, 2019). During stereotaxic procedures, mice were anesthetized using isoflurane (5 % induction, 1–2 % maintenance) and maintained normothermic by means of a feedback-controlled heat blanket (Harved Apparatus Ltd, Kent, UK). The depth of the anaesthesia was frequently tested by checking the plantar nociception or corneal reflex. Additionally, to minimize pain during and post-surgery, mice were treated with buprenorphine (0.05 mg/kg), and EMLA cream (Aspen Pharma, UK) which was applied to head wounds and ear bars. Once fully anesthetized, mice were placed in a stereotaxic frame and a midline scalp incision was performed to expose the skull. A guide cannula for IAKA injection (coordinates from Bregma; AP = -0.94 mm, L = -2.85 mm) and three cortical electrodes (IAKA and i.p. KA), one on top of each hippocampus and the reference electrode on top of the frontal cortex, were fixed in place with dental cement. For IAKA-induced SE, approximately 1 h post-surgery, SE was induced in awake, hand-restrained mice by a microinjection of 0.3 μg KA in 0.2 μl phosphate-buffered saline (PBS) (Sigma-Aldrich, Dublin, Ireland) into the right basolateral amygdala. All vehicle-injected control animals received 0.2 μl of PBS (pH = 7.4) solution. The anticonvulsant lorazepam (6 mg/kg) (Wyetch, Taplow, UK) was delivered i.p. 40 min following IAKA or vehicle to curtail seizures and reduce morbidity and mortality. Post-SE, mice were evaluated using a scoring sheet for scoring endpoints in rodents, approved by the HPRA, and the mouse Grimace scale. Mice were killed via cervical dislocation by a trained individual, if not otherwise indicated. For i.p. KA-induced SE, mice were injected with 10 mg/kg KA. Electroencephalogram (EEG) was recorded using a Xltek recording system (Optima Medical Ltd, Guildford, UK) starting 10 min before administration of IAKA or i.p. KA. For the induction of generalized tonic-clonic seizures, mice were treated i.p. with 60 mg/kg Pentylenetetrazol (PTZ). Mice were observed for 30 min post-PTZ administration.

2.4. Analysis of seizure severity and epilepsy

Behavioral seizures during IAKA and i.p. KA-induced SE were scored according to a modified Racine Scale as reported previously (Jimenez-Mateos, 2012). Score 1, immobility and freezing; score 2, forelimb and or tail extension, rigid posture; score 3, repetitive movements, head bobbing; score 4, rearing and falling; score 5, continuous rearing and falling; score 6, severe tonic-clonic seizures. The highest score attained during each 5 min period was recorded by an observer blinded to treatment. In the PTZ model, behavioral seizures were classified as: Score 0, normal behaviour; score 0.5, abnormal behaviour; score 1, isolated myoclonic jerk; score 2, atypical clonic seizure; score 3, bilateral forelimb clonus; score 3.5, bilateral forelimb clonus with body twist; score 4, tonic-clonic seizure with suppressed tonic phase; score 5, fully developed tonic-clonic seizure; score 6, tonic-clonic seizure followed by death. To analyze EEG frequency and amplitude signal (power spectral density and EEG spectrogram of the EEG data), EEG data were uploaded into Labchart7 software (AD instruments Ltd, Oxford, UK) and analyzed as before (Engel, 2018). EEG total power (μV^2) is a function of EEG amplitude over time and was analyzed by integrating frequency bands from 0 − 100 Hz and the amplitude domain filtered from 0 − 50 mV (Alves et al., 2018). Epilepsy analysis was carried out via continuous video monitoring. Animals were housed in pairs (mice were distinguished by different colors of headset) in clear Perspex cages. Webcam-style cameras connected to laptop computers were placed in front of each cage in a room equipped with safe lights for night-time recordings. Images were captured using VirtualDub 1.9.11 (SourceForge.net) with a sampling rate of 10 frames per second and data transfer rate of 140 kb s^{-1}. Videos were reviewed by an observer unaware of experimental treatment.

2.5. Tamoxifen treatment

Tamoxifen was used to induce the expression of Cre (*Cx3cr1* and *Thy-1*) to delete the P2X7R in either microglia ($P2rx7^{-/-}$-M) or neurons ($P2rx7^{-/-}$-N). This treatment was applied for a period of 7 consecutive days by an i.p. injection of tamoxifen once daily (40 mg/kg; prepared in 10 % of 100 % ethanol and 90 % of peanut oil; volume injection = 100 μl). For experiments with cell type-specific KO mice, animals negative for Cre but homozygous for loxP were used as controls ($P2rx7^{fl/fl}$). All mice received the same tamoxifen treatment regime.

2.6. Adeno-associated virus transduction

We used the adeno-associated virus (AAV) serotype 8, where the enhanced green fluorescent protein (eGFP) was either expressed alone (AAV-mDLXp-eGFP) (GFP^{Dlx} mice), or fused to the C-terminal of the mouse P2X7 (splice variant A) (AAV-mDLXp-mP2X7-eGFP; P2X7-overexpression$(OE)^{Dlx}$ mice) under the mDlx promoter thereby driving the expression towards GABAergic interneurons (Vector Biolabs, Malvern, PA, USA) (Dimidschstein, 2016). For AAV injections (GFP^{Dlx} or P2X7-OE^{Dlx}), fully anaesthetized mice were placed on a stereotaxic frame and a guide cannula was implanted (coordinates from Bregma; AP = -1.7 mm, L = -1.2 mm) and fixed in place with dental cement. AAVs were injected bilaterally in both hippocampi at a volume of 0.2 μl (titer: 1.0 x 1013 GC/ml) into the hippocampus (depth = 2 mm from Bregma). F1. *Scn1a*$(+/-)^{tm1Kea}$ mice were injected intracerebroventricular (i.c.v., 2 μl) at P10 with AAV-mDLXp-eGFP or AAV-mDLXp-mP2X7-eGFP using the following coordinates from Bregma (AP = 0 mm, L = 1 mm and depth = 2 mm).

2.7. Prolonged febrile event (PFE)

The PFE paradigm was adapted and optimised from (Dutton, 2017) to model an early-life complex febrile seizure event in F1.*Scn1a* $(+/-)^{tm1Kea}$ Dravet syndrome mice. At P17, mice previously injected at P10 with GFP^{Dlx} or P2X7-OE^{Dlx} AAV virus, were gently hand-restrained in a supine position with the tail lifted. Then, a temperature probe (RET-4, physitemp), covered with Vaseline, was inserted into the rectum and

taped on the tail, to keep it in place throughout the procedure. Ears were protected with a tape to later be placed into a Plexiglas box with an infrared heat lamp (HL-1, physitemp, Clifton, New Jersey) positioned above and the rectal probe attached to a TCAT-2DF thermocontroller (physitemp, Clifton, New Jersey). Each mouse was held at 37.5 °C for 5 min to become accustomed to the chamber. Later, core body temperature was gradually elevated by 0.5 °C every 2 min until 41 °C was reached (raising phase). This core body temperature was then maintained for 30 min (holding up phase). If the core temperature of the mouse transiently exceeded 41.3 °C during the PFE, the heat lamp was rapidly switched off to allow the core temperature return to 41 °C. Following the holding-up phase, and before returning the mouse to the home cage, the heating process was stopped by cooling down their body temperature to 37 °C on a cold surface. Outcome measures included the temperature threshold for the first seizure, total number of seizures, duration, and seizure severity. All seizures were video recorded to be further reviewed offline to characterize the behavioral seizures. Seizure severity was classified according to a modified Racine scale. No behavior changes (0), mouth and facial movements (1), head nodding (2), unilateral forelimb clonus (3), bilateral forelimb clonus with rearing (4), rearing and falling (loss of posture) (5), wild running or jumping (6) and tonic hindlimb extension followed or not by death (7).

2.8. Open field test

Mice were placed in an arena made of four transparent Plexiglas walls (30 x 30 x 30 cm) for a 10 min session and then returned to their home cages (Engel, 2013). The arena was cleaned with 70 % ethanol and water between sessions. Behavioural tests were recorded using an overhead Logitech Webcam C270 (720p) and different parameters including total distance travelled, total time mobile and total time in the center zone were analysed automatically with the ANY-maze video tracking system (Version 6.32).

2.9. RNA extraction and qPCR

RNA extraction was performed using the Trizol method (Alves, 2019). Quantity and quality of RNA was measured using a Nanodrop Spectrophotometer (Thermo Scientific, Rockford, IL, U.S.A). Samples with a 260/280 ratio between 1.8–2.0 were considered acceptable. 500 ng of total RNA was used to produce complementary DNA (cDNA) by reverse transcription using SuperScript III reverse transcriptase enzyme (Invitrogen, CA, U.S.A) primed with 50 pmol of random hexamers (Sigma, Dublin, Ireland). Quantitative real-time polymerase chain reaction (qPCR) was performed using the QuantiTech SYBR Green kit (Qiagen Ltd, Hilden, Germany) and the LightCycler 1.5 (Roche Diagnostics, GmbH, Mannheim, Germany). Each reaction tube contained 2 µl cDNA sample, 10 µl SyBR green Quantitect Reagent (Qiagen Ltd, Hilden, Germany), 1.25 µM primer pair (Sigma, Dublin, Ireland) and RNAse free water (Invitrogen, CA, U.S.A) to a final volume of 20 µl. Using LightCycler 1.5 software, data were analyzed and normalized to the expression of *β-actin*. Primers used (Sigma, Dublin, Ireland) are listed in Supplementary Table 1.

2.10. RNA sequencing

RNA sequencing was carried out by omiics.com (Aarhus, Denmark). Whole hippocampi were removed 8 h post-IAKA (or vehicle) from male wt and *P2rx7*$^{-/-}$ mice and RNA extracted as described above and stored at −80 °C. Samples ($n = 5$ per group) (each sample represented a pool of two hippocampi from two independent mice) were then shipped to the company on dry ice and sequenced as described. Samples were rRNA depleted and prepared for sequencing using SMARTer Stranded Total RNA Sample Prep Kit − HI Mammalian (Takara). In brief, this kit first removes ribosomal RNA (rRNA) using RiboGone technology and specifically depletes nuclear rRNA sequences (5S, 5.8S, 18S, and 28S) and mitochondrial rRNA 12S. RiboGone oligos are hybridized to rRNA, which is cleaved using RNase H mediated cleavage. First strand synthesis is performed using random priming, adding an anchor for use with later PCR steps. Template switching is utilized during the RT step and adds additional non-templated nucleotides to the 3′ end of the newly formed cDNA. PCR is performed leveraging the non-templated nucleotides and the added anchor sequence to produce Illumina compatible libraries. Prepared libraries were quality controlled using the Bioanalyzer 2100 (Agilent) and qPCR-based concentration measurements. Libraries were equimolarly pooled and sequenced including 20 % PhiX in-lane control as 150 bp paired end reads on a s4 lane of an Illumina NovaSeq 6000 sequencer.

2.11. RNA sequencing data processing and analysis

The analysis of RNA-seq data was performed using R language. Raw counts were inputted to the DESeq2 (Love et al., 2014) for calculation of differentially expressed genes (DEGs). No covariate was used in the generalized linear model. Significant DEGs were considered for FDR < 0.05. Variance Stabilization Transformation (VST) and normalized count values were used for Principal Component Analysis (PCA) and heatmap representations, respectively. Gene ontology (GO) enrichment was calculated using the enrichGO function from the clusterProfiler package (Wu, 2021), with the default full transcriptome as background. Evaluation of transcription factor (TF) enrichment was performed using regulon A reference data from Discriminant Regulon Expression Analysis (DoRothEA) (Garcia-Alonso, 2019), and the viper package (Alvarez, 2016), which uses lists of genes ranked by logFC and adjusted p value (FDR) of differential expression to calculate TF activities. The percentages of contribution of glutamatergic and GABAergic neurons, and non-neuronal cells within the bulk RNA-seq samples in our study were calculated using the deconvolution module from the BayesPrism algorithm (Chu, 2022). As reference we used a single-cell (sc)RNA-seq dataset developed on cortex and hippocampus of approximately 8-week-old mice developed using SMART-Seq v4 technology, and consisting of 73,363 cells (Yao, 2021). The data was downloaded from https://portal.brain-map.org/atlases-and-data/rnaseq/mouse-whole-cortex-and-hippocampus-smart-seq, and the original annotation based on subclass and class (Glutamatergic, GABAergic, and Non-Neuronal) was maintained and used for deconvolution. For visual representation, we used the ggplot2 package (Wickham, 2016), and for heatmaps, we used the heatmap.2 and Heatmap functions from the gplots (Warnes et al., 2022) and ComplexHeatmap (Gu et al., 2016) packages.

2.12. Analysis of human single-cell sequencing datasets

Analyses were performed on human single-nuclei sequencing data (snRNA-Seq) from the temporal cortex of 9 TLE patients and 10 autopsy controls. Filtered count matrices were obtained from (Pfisterer, 2020). All plotting and analyses were done in R using code adapted from https://github.com/khodosevichlab/Epilepsy19. Assignment of neuronal subtypes to individual cells was performed as in (Pfisterer, 2020). Joint graphing of single-cells was performed using Conos v.1.5.0 (Barkas, 2019). Normalization of the gene expression counts and pseudobulk differential expression analysis were done using DESeq2 v1.40.1. Code is available at https://github.com/Javizuma/P2RX7_analysis.

2.13. Laser capture microdissection (LCM)

Brains were removed from PBS-perfused tamoxifen-treated *P2rx7*$^{-/-}$-N and corresponding wt mice (*P2rx7*$^{fl/fl}$) 40 min post-IAKA and frozen in dry ice. 12 µm thick coronal sections at the medial level of the hippocampus (Bregma AP = -1.94 mm) were cut on a cryostat and placed on enhanced adhesion 2.0 µm PEN-membrane slides (MicroDissect GmbH, Herborn Germany). Using a ZEISS PALM MicroBeam equipped with a Fluar 5x/0.25 objective, PALM CapMover and PALMRobo software V4.9

(Carl Zeiss, Germany), cornu Ammonis 3 (CA3) hippocampal subfield from 9 different slices of the same mouse were laser pressure catapulted into a 500 µl Eppendorf containing trizol reagent. Samples were then processed to extract RNA and analysed by qPCR.

2.14. Western blotting

Western blot analysis was performed as described (Engel, 2013). Lysis buffer (100 mM NaCl, 50 mM NaF, 1 % Tx-100, 5 mM EDTA pH 8.0, 20 mM HEPES pH 7.4) containing phosphatase and protease inhibitors was used to homogenize brain tissue and extract proteins, which was quantified using a Tecan plate reader at 560 nm. 30–50 µg of protein per sample was loaded onto an acrylamide gel and separated by sodium dodecyl sulphate–polyacrylamide gel electrophoresis (SDS-PAGE). Following electrophoresis, proteins were transferred to a nitrocellulose membrane (GE Health Care) and immunoblotted with primary antibodies (Supplementary Table 2). Membranes were incubated with horseradish peroxidase-conjugated goat anti-rabbit or anti-mouse secondary antibodies (1:5000; Sigma-Aldrich, Dublin, Ireland). Protein bands were visualized using Fujifilm LAS-4000 system with chemiluminescence (Imombilon western HRP substrate, Merck Millipore, Cork, Ireland) followed by analysis using Alpha-EaseFC4.0 software. Spot dense option was used to evaluate the optical density of each protein band. Protein quantity was normalized to the loading control β-Actin (1:1000; anti-mouse; Sigma-Aldrich, Wicklow, Ireland) or GAPDH (1:1000; anti-rabbit; Cell-signalling, Massachusetts, USA).

2.15. Immunofluorescence

Mice were transcardially perfused with PBS followed by 4 % paraformaldehyde (PFA) and brains removed. Following 24 h of post-fixation in 4 % PFA at 4 °C, brains were transferred to PBS and immersed into 4 % agarose. 50 µm sagittal sections were cut using the VT1000S vibratome (Leica Biosystems, Wetzlar, Germany) and sections were stored at −20 °C in glycol. Tissue sections were incubated with 0.1 % triton/PBS, followed by 1 M glycine and with 1 % BSA-PBS. Sections were then incubated with primary antibodies overnight (Supplementary Table 2). After washing in PBS, tissue was incubated with fluorescent secondary antibodies, AlexaFluor-568 (Cat #: A-11011) or −488 (Cat #: A11008) (1/400 prepared in 1 % BSA-PBS; anti-rabbit-IgG; BioSciences, Dublin, Ireland), followed by a short incubation with DAPI (1:500; Sigma-Aldrich, Dublin, Ireland). FluorSave™ (Millipore, Dublin, Ireland) was used to mount tissue. Confocal images were taken with a Zeiss 710 LSM NLO confocal microscope equipped with four laser lines (405, 488, 561, and 653 nm) using a 40X immersion oil objective and ZEN 2010B SP1 software. For immunofluorescence using P2X7R nanobodies (Kaczmarek-Hajek, 2018), tissue sections were washed with PBS, then washed in 0.1 % triton-X100 for 7 min and blocked with 0.05 % saponin/3% BSA/15 mM NH_4Cl/PBS (blocking buffer) for 20 min. Primary antibodies against P2X7R (1:200; anti-rabbit nanobody; Nolte group, Hamburg, Germany) and GFP (1:400; anti-chicken, Invitrogen, Waltham, Massachusetts, USA) were incubated overnight at 4 °C in blocking buffer without saponin. After 3 washes with PBS, sections were incubated for 2 h at room temperature (RT) with secondary antibodies, AlexaFluor-488 and AlexaFluor-647 (1:400; Life Technologies, Eugene, Oregon, USA), washed 3 times with PBS, shortly stained with DAPI (1 mg/L, Carl Roth, Karlsruhe, Germany), washed with water and mounted (PermaFluor, Thermo Fisher, Dreieich, Germany) for confocal microscopy on a Zeiss LSM880 equipped with four laser lines (405, 488, 561 and 633 nm) using a 40X immersion oil objective and ZEN 2.3 SP1 FP1 (black) software.

2.16. 3D morphological analysis of microglia

To analyse morphological changes of microglia, we performed an immunofluorescence staining, as described in the previous section. Microglia cells were identified via Iba-1 (1:400; anti-goat; Abcam, Cambridge, UK). Z-stacks of ≈ 450 slices (~15 µm thickness) were taken with a Zeiss 710 LSM NLO confocal microscope using a 40x immersion oil objective and ZEN 2010B SP1 software. Z-stacks were taken from each hippocampal subfield (*i.e.*, CA1, CA3 and DG), amounting to 3 images per slice, $n = 3$ per group (Control) and $n = 3$ per group (SE) for both $P2rx7^{fl/fl}$ and $P2rx7^{-/-}$-M mice. Images were subsequently rendered in 3D using FluoRender Version 2.25.0. Three cells from each subfield were selected at random by a reviewer blind to groups, and were isolated from the z-stack. Once isolated, background signal was removed using the 'threshold slider'. Cell process length was then measured on the same software, using the multipoint measurement tool, beginning from the border of the soma (located using DAPI) to the most extremity of the cell process. Only primary processes were analyzed, meaning processes that extended directly from the soma, as opposed to secondary or tertiary processes branching of the primary cell process. Average process length was calculated as the mean length of all primary processes extending from the cell body of each individual cell.

2.17. Immunofluorescence and VGAT- and VGLUT-positive puncta quantification analysis

Brain sections (50 µm thick) were blocked for 1 h in phosphate buffer (PB) (0.1 M) with 0.25 % Triton X-100 and 3 % normal goat serum (Vector Laboratories Inc., Burlingame, CA, USA), and then incubated at 4 °C overnight in the same solution with primary antibodies (Supplementary Table 2). After rinsing in phosphate buffer (PB), sections were incubated for 2 h at RT with biotinylated goat anti-guinea pig antibody (1:200, BA-7000, Vector) and finally 2 h at RT with streptavidin coupled to AlexaFluor-594 (1:1000, S-32356, Molecular Probes). Then, sections were rinsed in PB, counterstained with DAPI, and coverslipped with ProLong Gold antifade reagent (Life Technologies, Carlsbad, CA). For VGAT- and VGLUT-positive puncta quantification, confocal image stacks were taken with a Zeiss LSM880 confocal microscope and ZEN 2010B SP1 software equipped with three laser lines (405, 488 and 561 nm). The fluorescence of DAPI, and AlexaFluor-488 and AlexaFluor-954 were recorded through separate channels. Images were acquired using a 63x immersion oil objective with pinhole aperture set to 5.76 Airy Unit and pixel size of 70x70x140 nm. Five pictures per mouse were acquired from the dentate gyrus (DG) region of the hippocampus. Image intensity normalization and VGAT / VGLUT spot counting were performed in ImageJ using the spot segmentation procedure implemented in 3D ImageJ Suite plugins (http://imagejdocu.tudor.lu/doku.php?id=plugin:stacks:3d_ij_suite:start) (Gilles, 2017). For spot segmentation, the following parameters were used: Maxima detection: radius in xy-axis = 2, in z-axis = 3, noise parameter set to zero; threshold for maxima selection was set to 28000; Parameters for Gaussian fit and threshold calculation were Radius maximum = 10, S.D. value = 1.5. After acquisition, stacks were coded to randomize the experimental conditions and these codes were not revealed until quantitative analysis had been completed. All analysis was performed by the same investigator.

2.18. Diaminobenzidine staining

Diaminobenzidine staining (DAB) was carried out as reported (Engel, 2018). Mice were perfused with 4 % PFA, brains post-fixed for 24 h, and 30 µm sagittal sections were cut on a Leica cryostat. Next, brain sections were pretreated for 1 h with 1 % bovine serum albumin, 5 % fetal bovine serum, and 0.2 % Triton™ X-100 followed by an overnight incubation with primary antibody (Supplementary Table 2). Next, brain sections were incubated in avidin–biotin complex using the Elite® VECTASTAIN® kit (Vector Laboratories). Chromogen reactions were performed with diaminobenzidine and 0.003 % hydrogen peroxide for 10 min. Sections were coverslipped with Fluorosave™.

2.19. Histopathology

Sections from the same brains analysed for neurodegeneration using FjB, were fixed in 4 % PFA which was followed by permeabilization with 3 % Triton and blocking with 5 % goat serum. Sections were then incubated overnight with the specific cell type markers (Supplementary Table 2). After rinsing with PBS, slices were incubated with secondary antibodies conjugated to AlexaFluor-568 (Cat #: A-11011) or −488 (Cat #: A11008) (1/400 prepared in 5 % goat serum; anti-rabbit-IgG; Bio-Sciences, Dublin, Ireland) for 2 h at RT, followed by DAPI incubation. Sections were mounted using FluorSave (Merck Millipore, Massachusetts, USA) and two images from each hippocampal subfield were obtained using a 40x lens in the Nikon 2000 s epifluorescence microscope. The number of cells was counted by a person unaware of treatment and results presented by the average counting of two images.

2.20. Fluoro-Jade B staining

12 μm coronal sections at the medial level of the hippocampus (Bregma AP = -1.94 mm) were cut on a cryostat. Tissue was fixed in formalin, rehydrated in ethanol, and then transferred to a 0.006 % potassium permanganate solution followed by incubation with 0.001 % FjB (Chemicon Europe Ltd, Chandlers Ford, UK). Sections were mounted in DPX mounting solution. Then, using an epifluorescence microscope, cells including all hippocampal subfields (DG, CA1 and CA3 regions) were counted by a person unaware of treatment under a 40x lens in two adjacent sections and the average was determined for each animal.

2.21. Cytokine measurement in brain tissue

IL-1β, Tumor necrosis factor-α (TNF-α) and IL-10 levels were measured using the DuoSet ELISA kits from R&D Systems following the manufacturer's instructions (mouse IL-1β/IL-1F2, Cat #: DY401-05, mouse TNF-α, catalog #DY410-05, mouse IL-10 catalog #DY417-05). First, the detection antibody was incubated overnight in a 96-well ELISA plate at RT. Then, 100 μl of samples (50 ng) and standard curve (IL-1β: from 15.6 − 1000 pg/ml; TNF-α and IL-10: 31.2–2000 pg/ml) were added to wells and incubated for 2 h at RT, followed by incubation with 100 μl of streptavidin-HRP complex. A color reaction, caused by the addition of a substrate solution (100 μl) and terminated via stopping solution (50 μl), was quantified at 450 and 570 nm using a microplate reader. Cytokine concentration was obtained following the manufacturer's recommendations; 570 nm values were subtracted from the 450 nm values. The log10 of the standard curve values were plotted, and a line of best fit was generated. The amounts of cytokines were extrapolated using a standard curve and average of calculated triplicate. The cytokine concentration was then normalized to milligrams of total protein concentration in tissue. Data is presented as n-fold of control samples.

2.22. Ex vivo electrophysiology field recordings

SE was induced via IAKA in mice transduced with GFP-AAV^{Dlx} or P2X7R-AAV^{Dlx} two weeks post-transduction and allowed to continue for 40 min. After this time, mice were euthanized by cervical dislocation for ex vivo brain slice preparation. Brains were quickly dissected and submerged in oxygenated (95 % O_2 / 5 % CO_2) ice-cold sucrose artificial cerebrospinal fluid (S. aCSF; composition: in mM: 0.5 $CaCl_2$; 25 $C_6H_{12}O_6$; 7 $MgSO_4$; 1.25 NaH_2PO_4; 2.5 KCl; 25 $NaHCO_3$; 87 NaCl; 75 $C_{12}H_{22}O_{11}$). 400 μm horizontal slices were prepared using a vibratome (Campden 7000 smz II, Campden Instruments, Loughborough, UK), with bath temperature held at RT. Only slices from the hemisphere ipsilateral to IAKA injection were retained and stored at RT in a submerged-style holding chamber, filled with oxygenated recording aCSF (R. aCSF: in mM: 2.5 $CaCl_2$; 11 $C_6H_{12}O_6$; 1 $MgSO_4$; 1 NaH_2PO_4; 2.5 KCl_2; 26.2 $NaHCO_3$; 119 NaCl). Slices were equilibrated to these conditions for one hour prior to recording, when they were transferred to a membrane chamber perfused with oxygenated R. aCSF, heated to 34 °C, at a rate of 5 ml/min (47). A stimulating electrode (SS3CEA4-200, MicroProbes, MD, USA) was placed into the perforant pathway of the DG and 100 μs duration current pulses of varying amplitude were delivered using a DS3 isolated current stimulator (Digitimer, Welwyn Garden City, UK). Extracellular borosilicate glass recording electrodes (~3 MΩ) were made using an automatic electrode puller (PC-100, Narishige), filled with R. aCSF, and placed in the DG. A silver/silver chloride wire submerged in the bath was used as the bath earth to complete the circuit. Signals were acquired using a MultiClamp 700B amplifier (Molecular Devices, CA, USA), Power 1401 digitiser (Cambridge Electronic Design, Cambridge, UK) and Clampex software (11.2, Molecular Devices, CA, USA). Signals were digitized at 25 kHz and low pass filtered at 10 kHz. Data were analysed using Signal v6. Amplitude of fEPSP was measured and analyzed using Clampfit (11.2, Molecular Devices, CA, USA). Exposure for 40 min to Mg^{2+}-free modified aCSF (M. aCSF; in mM: 2.5 $CaCl_2$; 11 $C_6H_{12}O_6$; 1 NaH_2PO_4; 2.5 KCl_2; 26.2 $NaHCO_3$; 119 NaCl) was used to induce epileptiform activity in hippocampal slices. Stocks of GABA antagonists were prepared in advance as per manufacturer's guidelines, kept at −20 °C, and diluted to the following final concentrations in the circulating aCSF during electrophysiological recordings: CGP 55845 hydrochloride (Tocris, UK) selective $GABA_B$ receptor antagonist (5 μM); Bicuculline methochloride (Alomone, Ireland) competitive $GABA_A$ receptor antagonist (10 μM).

2.23. Patch-clamp recordings

Ipsilateral brain hemispheres were extracted from AAV-transduced mice 14 d post-IAKA/vehicle, and attached to an agarose cube and placed on the stage of a vibratome cuvette (Integraslice 7550, Campden Instruments, UK) filled with a Mg^{2+}-free and low-Ca^{2+} saline solution (125 mM NaCl, 2.5 mM KCl, 1 mM $CaCl_2$, 1.25 mM NaH_2PO_4, 26 mM $NaHCO_3$, and 12 mM glucose, pH 7.4, ~300 mOsm) at 4 °C. Brain slices (300 μm thickness) were obtained by sectioning through the sagittal plane, and subsequently kept in saline solution continuously bubbled with carbogen (95 % O_2/5% CO_2) at RT for a maximum of 6 h. Patch-clamp recordings were performed in brain slices placed in a superfusion chamber attached to the stage of an upright microscope (BX51W1, Olympus, Japan) and connected to a gravity-driven perfusion system, which delivered the above-mentioned saline solution at a rate of 2 ml/min. A 63X water-immersion objective with fluorescence illumination and a DL-604 OEM camera (Andor Technology, UK) was used for hilar GFP-positive interneuron visualization. Patch pipettes were made from borosilicate capillaries (Kimble Chase, Mexico) with a programmable puller (Narishige PP830, Japan) to a final resistance of 5–6 MΩ when filled with the intracellular solution (140 mM, N-methyl-D-glucamine ($NMDG^+$), 5 mM EGTA, 3 mM $MgCl_2$, 10 mM HEPES, pH 7.2, ~290 mOsm). Whole-cell membrane currents were measured with an EPC10/2 patch-clamp amplifier using PatchMaster software (HEKA Elektronik, Germany) in cells held at a voltage of −70 mV, filtered at 3 kHz and sampled at 10 kHz. Series resistance was compensated by 80 % and monitored throughout the experiment together with the cell membrane capacitance. Experiments in which series resistance changed by ~ 20 % or in which holding current exceeded 20 pA were not analysed. BzATP (100 μM; Sigma-Aldrich) was applied onto recorded cells via separated glass pipettes (3–5 μm tip diameter) connected to a pneumatic drug ejection system (PDES-02DX, NPI Electronic, Germany). At variance, the P2X7R antagonist A438079 (10 μM; Sigma-Aldrich) was administered through perfusate, 2 min before and during BzATP application.

2.24. Primary cell cultures and calcium imaging

Whole brain without the cerebellum from postnatal day 3 mouse pups were incubated with papain, mechanically dissociated, and plated

at 500 cells/mm^2 on Geltrex-coated glass coverslips in culture medium consisting of neurobasal medium with 2 % B-27 supplement, 1 % L-glutamine, 1 % nonessential amino acids and 10 % FCS (Thermo Fisher Scientific, Massachusetts, USA). Cultures were maintained at 37 °C in a humidified incubator. Cytosine arabinoside at 1 mM was added 3 days after plating to inhibit glial proliferation. Media was replaced every 3–4 days. Viral transduction was performed at 6 days and cells were used for experiments at 14–15 DIV. Prior to imaging, cultures were loaded with 2 μM cell-permeant cal-590 AM calcium indicator (Biotium, CA, USA) and incubated for 45 min. Cells were, then, washed several times with dye-free HEPES-buffered saline solution and transferred to an imaging chamber on a microscope (Zeiss Axio Examiner, Jena, Germany) equipped with a Zeiss 40x water immersion objective. Zen Blue imaging software (Carl Zeiss, Jena, Germany) was used for hardware control and image acquisition, and image analysis was performed using ImageJ (NIH, Maryland, USA). All imaging experiments were performed at 32 °C in a low divalent cation-containing bath solution with the composition (in mM): 135 NaCl, 3 KCl, 0.1 $CaCl_2$, 0 $MgCl_2$, 10 HEPES, 300 nM TTX and 10 glucose (pH 7.2; osmolality 290–300 mmol/kg). Images were acquired at 4 Hz.

2.25. Fluorescence-Activated cell sorting (FACS)

Hippocampi were dissected from tamoxifen-treated *P2rx7*$^{-/-}$-M and *P2rx7*$^{fl/fl}$ mice. Cells were dissociated using the Worthington Papain Dissociation System (cat no LK003153) following the instructions of the manufacturer: the dissected tissue was placed in papain solution (composed of papain, 5 ml Earle's balanced salt solution (EBSS) and 250 μl DNAseI) and incubated for up to 60 min at 37 °C with constant agitation. Next, mechanical trituration was performed with a sterile Pasteur pipette and the cloudy cell suspension was placed in a sterile 15 ml tube and centrifuged at 300 × g for 5 min at RT. The cell pellet was re-suspended in 108 ml EBSS with 12 μl reconstituted albumin-ovomucoid inhibitor solution and 6 μL DNaseI, layered on top of 200 μl albumin-inhibitor solution, then centrifuged at 70 × g for 6 min at 4 °C. The cell pellet was re-suspended in 300 μl PBS in 0.4 % BSA and centrifuged at 70 g for 5 min at 4 °C. This was done twice, and the resulting pellet was resuspended in blocking solution composed of 50 μl of PBS with 0.5 μl of CD16/CD32 (unspecific antibody) and incubated for 15 min on ice. Then, 50 μl of PBS with 0.5 μl of CD11b (microglia) and 0.5 μl of CD45 (macrophages) was added, and cells were incubated for an additional 15 min. Finally, cells were resuspended in 1 ml of PBS and centrifuged at 1400 x rpm for 7 min at 4 °C. The cell suspension was filtered using Bundle pluriStrainer® Mini 70 μm (cat no 43–10070-46). CD11b- and CD45-positive cells were sorted and acquired on a FACSAria Fusion (BD Biosciences) cell sorter, with purity > 95 %. Analysis was performed using FlowJo software.

2.26. Statistics

Statistical design of experiments can be found in the "Results" section in Figure Legends including control groups, group size and statistical test used. Statistical analysis of data was carried out using GraphPad Prism 8 and STATVIEW software (SAS Institute, Cary, NC, U.S.A). Data are presented as means ± standard error of the mean (SEM). One-way ANOVA parametric statistics with *post hoc* Fisher's protected least significant difference test or Turkey post-hoc test was used to determine statistical differences between three or more groups. Unpaired Student's *t*-test (parametric) or non-parametric Mann-Whitney was used for two-group comparison. Two-way ANOVA was used for repeated measures between groups where a series of measurements have been taken from the same mouse at different time-points. Normality and lognormality test were used to verify the normal distribution between groups. Significance was accepted at $^*P < 0.05$.

3. Results

3.1. Status epilepticus in mice lacking the P2X7R alters glial and neuronal gene expressions in the hippocampus

To gain first unbiased insights into the cellular signaling of P2X7R activity during seizures, we subjected wild-type (wt) and *P2rx7*$^{-/-}$ mice to IAKA. IAKA leads to convulsive SE, attendant neurodegeneration and gliosis, and the development of epilepsy after 3–5 days (Engel, 2012; Mouri, 2008). Notably, gene changes in the IAKA mouse model have been shown to closely mimic the gene expression landscape observed in human TLE (Conte, 2020). RNA was extracted from the ipsilateral hippocampi of vehicle-injected control mice and mice subjected to IAKA-induced SE 8 h post-lorazepam administration and analysed via RNA sequencing (Fig. 1A). This time-point corresponds to when major seizure activity has ceased and precedes the appearance of wide-spread neuronal death (Alves et al., 2019). Of note, no difference in seizure severity was observed between genotypes during SE, although *P2rx7*$^{-/-}$ mice responded slightly better to lorazepam when compared to wt mice (Supplementary Fig. 1A-E), as reported previously (Beamer, 2022; Conte, 2020). Genes were considered differentially expressed between conditions and genotypes when the adjusted *P*-value (FDR) was ≤ 0.05.

As expected, the most up-regulated genes in wt mice 8 h post-IAKA, when compared to wt control mice, included activity-dependent transcripts such as *Bdnf*, *Arc*, *c-Fos* and early markers of glial response such as *Gfap* (Supplementary Table 3). A Principal Component Analysis (PCA) plot accounting for the whole transcriptome shows that the highest degree of variance (PC1: 77 %) relates to the induction of SE, whereas PC2 (9 % variance) is explained by the KO of *P2rx7* (Fig. 1B). Moreover, the degree of variance caused via the deletion of *P2rx7* was higher post-SE when compared to controls, in line with P2X7R requiring pathological conditions (*i.e.*, SE) to be activated (Surprenant, 1996). Differentially expressed genes (DEGs) were calculated for each pairwise comparison between all four studied groups, outputting 12,597 unique genes (Supplementary Table 3). Next, unsupervised hierarchical clustering grouped the list of DEGs in six gene clusters (Fig. 1C and Supplementary Table 4). Similar gene expression was observed between genotypes during baseline conditions in all 6 clusters. Gene expression differed, however, between control and post-SE with clusters 1–3 showing an overall downregulation and clusters 4–6 showing an overall up-regulation (Fig. 1C). We next compared gene expression between genotypes post-SE. While cluster 1 and 2 show an overall decreased expression pattern for both genotypes post-SE, cluster 5 and 6 show an overall increased expression profile post-SE for both wt and *P2rx7*$^{-/-}$ mice (Fig. 1C). Notably, cluster 3 showed a decrease in gene expression in post-SE versus control exclusively in wt mice, being absent or attenuated in *P2rx7*$^{-/-}$ mice. Conversely, cluster 4 showed increased gene expression in post-SE versus control only for wt mice and not for *P2rx7*$^{-/-}$ mice, which showed similar gene expression levels when compared to control conditions (Fig. 1C).

We next investigated which biological pathways are altered in *P2rx7*$^{-/-}$ mice focusing on cluster 3 and 4. Pathways identified in cluster 3 include genes involved in axonal growth, synapse formation and myelination, processes previously associated with P2X7R signaling (Diaz-Hernandez, 2008; Otrokocsi et al., 2017; Bernal-Chico, 2020). Gene pathways identified to be down-regulated in *P2rx7*$^{-/-}$ mice when compared to wt mice post-SE in cluster 4 include myelination, cytosolic transport, GTPase activity, involved in membrane trafficking, and the regulation of cytokine stimulus (Fig. 1D and Supplementary Fig. 2), in line with P2X7R promoting proinflammatory signaling (Di Virgilio, 2017). Of note, gene pathways identified in cluster 6 including pro-inflammatory pathways (*e.g.*, regulation of immune response, regulation of cytokine production) were found up-regulated in both genotypes, suggesting inflammatory responses are only partially suppressed in *P2rx7*$^{-/-}$ mice post-SE (Fig. 1D).

To identify transcription factors (TFs) potentially implicated via

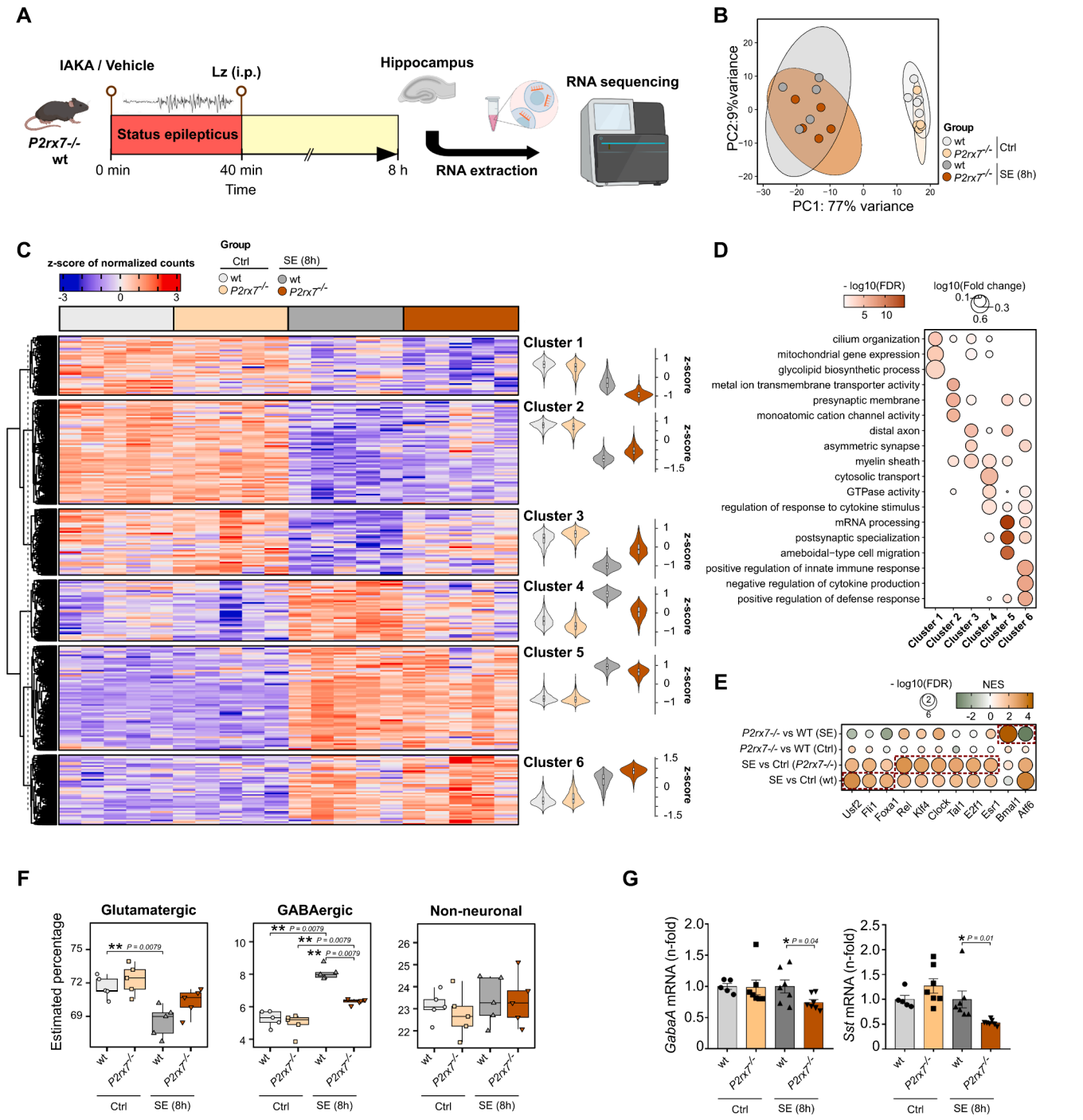

Fig. 1. RNA sequencing in the hippocampus of P2X7R KO mice. (A) RNA sequencing was carried out using the ipsilateral hippocampus from wt and *P2rx7*$^{-/-}$ mice, taken 8 h after the injection of intraamygdala vehicle or KA. Ipsilateral hippocampi were processed for RNA extraction and sent for RNA-sequencing analysis. (B) Principal Component Analysis (PCA) plot accounting for the whole transcriptome showing that the highest degree of variance (PC1: 77 %) relates to the induction of status epilepticus (SE), whereas PC2 (9 % variance) is explained by the knock-out of *P2rx7*. The degree of variance caused by *P2rx7* knock-out was higher post-SE than under control conditions. (C) Heatmap representation of the z-score of the normalized counts of all pairwise differentially expressed genes (DEGs) between the four studied conditions (FDR < 0.05), grouped in six clusters with unsupervised hierarchical clustering. The violin plots represent the mean of the z-score by group for each DEGs. (D) Dotplot representation of a selected list of enriched gene ontology (GO) terms for each of the DEG clusters. The selection was based on the statistical significance and biological relevance in the context of epilepsy and *P2rx7*. Significance is represented by the negative of the logarithm of the adjusted p value (FDR) and the logarithm of the fold change of the enrichment. (E) Dotplot representation of transcription factor (TF) enrichment for each of the transcriptomic pairwise comparisons. The red boxes highlight the TFs that are significantly enriched (FDR < 0.05) for a unique comparison. Significance is represented by the NES (Normalized Enrichment Score) and the negative of log of the adjusted *P* value (FDR). (F) Boxplot representation of the percentages of contribution of the glutamatergic and GABAergic neurons and non-neuronal cells in our bulk RNA-seq samples using the deconvolution module from BayesPrism and a single-cell (sc)RNA-seq dataset developed on mice whole cortex and hippocampus. Data are shown in the boxplots as mean ± 25th and 75th quartiles, and the hinges represent the highest and lowest values. (G) *GabaA* and *Sst* mRNA levels in the ipsilateral hippocampus of wt and *P2rx7*$^{-/-}$ mice 8 h post-SE. F, Wilcoxon–Mann–Whitney test. G, One-way ANOVA followed by Fischer's multiple-comparison test. Data are shown as mean ± SEM. **P* < 0.05, ***P* < 0.01. Created with BioRender.com. (For interpretation of the references to color in this figure legend, the reader is referred to the web version of this article.)

P2X7R, we performed regulon analysis (Garcia-Alonso, 2019). This showed that genes regulated via the TFs USF2, FLI1 and FOXA1 were up-regulated among DEGs post-SE in wt mice but not *P2rx7*$^{-/-}$ mice. In contrast, genes regulated via the TFs REL, KLF4, CLOCK, TAL1, E2F1 and ESR1 were up-regulated among DEGs in *P2rx7*$^{-/-}$ mice post-SE but not wt mice (Fig. 1E). Notably, genes regulated via the TF BMAL1 were found to be up-regulated among DEGs in *P2rx7*$^{-/-}$ mice and genes under the control of the TF ATF6 were down-regulated among DEGs in *P2rx7*$^{-/-}$ mice (Fig. 1E). Of note, *Atf6* deficiency has been shown to suppress microglia activation (Ta, 2016), further suggesting a pro-inflammatory function of the P2X7R.

So far, our sequencing results suggest P2X7R to be involved in the regulation of both non-neuronal (*e.g.*, inflammation, myelination) and neuronal (*e.g.*, axonal growth, synapses) pathways. To obtain further evidence of effects of P2X7R signaling on neuronal cell types, we used the deconvolution module from the BayesPrism algorithm, which allows us to estimate the proportions of contribution of different cell types within each bulk RNA-sequencing sample (Supplementary Table 3). To this end, we used a single-cell (sc)RNA-sequencing dataset developed on mice, which included the whole cortex and hippocampus (Yao, 2021). We estimated the percentages of the main annotated cell types, glutamatergic and GABAergic neurons and non-neuronal cells, and observed a significant decrease in the proportion of GABAergic neurons in *P2rx7*$^{-/-}$ in comparison to wt post-SE (Fig. 1F). For a selection of the neuronal genes, we validated the RNA sequencing results using qPCR, which confirmed altered expression (down-regulation) of selected GABAergic interneuron-specific genes (*Gabra1*($GABA_A$) and *Sst*) in *P2rx7*$^{-/-}$ mice post-SE (Fig. 1G).

In summary, P2X7R signaling post-SE seemed to be involved in glial responses, possibly contributing to SE-induced inflammation, and neuronal pathways, most prominently involving genes involved in GABAergic signaling.

3.2. Cell type-specific effects of the P2X7R on acute seizures and epilepsy

To obtain direct evidence that P2X7R expression on both microglia and neurons contributes to seizures during SE, we generated mice lacking the *P2rx7* in either microglia or neurons. Using the conditional Cre-LoxP system, we targeted the P2X7R in microglia by crossing *P2rx7*$^{fl/fl}$ mice with the *Cx3cr1*-Cre line, generating offspring, *P2rx7*$^{-/-}$-M. We generated mice lacking the P2X7R in neurons by crossing *P2rx7*$^{fl/fl}$ mice with the *Thy-1*-Cre line, generating the offspring *P2rx7*$^{-/-}$-N (Young, 2008; Sahasrabuddhe and Ghosh, 2022). Both lines used a tamoxifen-inducible Cre-LoxP system, thereby avoiding effects of P2X7R deficiency during development and allowing analysis of the loss of the P2X7R initiated after SE to track effects on epilepsy without interfering with the initial insult (Fig. 2A).

P2X7R deficiency in microglia post-tamoxifen was confirmed via FACS followed by qPCR, showing no *P2rx7* mRNA amplification in microglia ($CD11^+/CD45^-$) or macrophages ($CD11^-/CD45^+$) in *P2rx7*$^{-/-}$-M mice post-IAKA (Fig. 2B). Co-immunostaining using a highly specific P2X7R nanobody (Kaczmarek-Hajek, 2018) and the microglia marker Iba-1 further confirmed the absence of P2X7R on microglia, where P2X7Rs are normally highly expressed, in *P2rx7*$^{-/-}$-M mice subjected to IAKA post-tamoxifen treatment (Fig. 2C). Of note, P2X7R expression was still present on microglia in tamoxifen-treated *P2rx7*$^{-/-}$-N mice subjected to IAKA (Supplementary Fig. 3A). Analysis using laser capture microdissection (LCM) of the CA3 subregion of the hippocampus of wt and *P2rx7*$^{-/-}$-N mice confirmed the lack of *P2rx7* expression in CA3 neurons (Fig. 2D). qPCR of hippocampal tissue from *P2rx7*$^{-/-}$-N mice subjected to IAKA showed altered glutamatergic and GABAergic genes, suggesting *Thy-1*-Cre-mediated knock-out impacting on both glutamatergic and GABAergic neurons. Of note, while glutamatergic genes showed both up- and down-regulation when compared to *P2rx7*$^{fl/fl}$ mice post-SE, GABAergic genes seemed to be mainly down-regulated (Supplementary Fig. 3B). qPCR and Western blot confirmed that *P2rx7* mRNA and protein levels were reduced by ~ 20–40 % post-tamoxifen treatment in the hippocampus of *P2rx*$^{-/-}$-M and *P2rx7*$^{-/-}$-N mice under baseline conditions and following SE (8 and 24 h) (Fig. 2E-G).

To test whether a cell type-specific loss of the P2X7R impacts on the severity of seizures, *P2rx7*$^{-/-}$-M and *P2rx7*$^{-/-}$-N mice, along with wt controls (*P2rx7*$^{fl/fl}$) were subjected to IAKA (Fig. 2H). Compared to *P2rx7*$^{fl/fl}$ mice, *P2rx7*$^{-/-}$-M mice experienced reduced seizure severity as measured by surface EEG recordings during the 40 min following IAKA until administration of the anticonvulsant lorazepam (Fig. 2I, J). In contrast, *P2rx7*$^{-/-}$-N mice developed more severe seizures during IAKA-induced SE compared to *P2rx7*$^{fl/fl}$ animals (Fig. 2I, J). Tamoxifen-treated Cre-expressing mice (*i.e.*, *Cx3cr1* and *Thy-1*), that were not crossed with the *P2rx7*$^{fl/fl}$ line, showed either similar responses (*Thy-1*) or increased susceptibility (*Cx3cr1*) to IAKA, ruling out effects are due to Cre expression (Supplementary Fig. 4).

Analysis of brain samples 72 h post-SE revealed that *P2rx7*$^{-/-}$-N mice displayed increased neurodegeneration and astrogliosis when compared to *P2rx7*$^{fl/fl}$ mice. In contrast, *P2rx7*$^{-/-}$-M mice displayed similar levels of seizure-induced neuronal death and GFAP-positive cells in the hippocampus. No difference was observed in the number of Iba-1-positive cells across genotypes (Supplementary Fig. 5A-C).

To confirm the effects of cell type-specific deletion on seizures, we tested additional mice using the PTZ mouse model, a frequently used model to assess anti-or proconvulsant effects (Löscher, 2017) (Fig. 2K). Consistent with the earlier findings in the IAKA model, *P2rx7*$^{-/-}$-N mice developed more severe behavioral seizures when compared to *P2rx7*$^{fl/fl}$ mice and *P2rx7*$^{-/-}$-M mice, whereas *P2rx7*$^{-/-}$-M mice displayed a delay to the first myoclonic tonic-clonic seizure (Fig. 2L-N). Moreover, all *P2rx7*$^{-/-}$-M survived the first 30 min post-PTZ injection compared to only ~ 70 % of *P2rx7*$^{fl/fl}$ mice and approximately 50 % of *P2rx7*$^{-/-}$-N (Fig. 2O). These findings suggest that the cell type-specific effects of deleting the P2X7R from neurons or microglia are independent of the method of seizure induction.

To determine if the disruption of P2X7R signaling in microglia or neurons affects the IAKA-induced epileptic phenotype, additional mice of each genotype were treated with tamoxifen beginning 24 h after IAKA-induced SE (Fig. 2P). Using this approach, the deletion of P2X7R occurred after SE without impacting the initial insult (*i.e.*, SE). Deletion of the P2X7R in microglia reduced the number of spontaneous seizures in mice during a 14-day recording period when compared to *P2rx7*$^{fl/fl}$ mice, starting at 3 days post-SE. In contrast, the absence of *P2rx7* expression from neurons resulted in a slightly more severe epilepsy phenotype when compared to *P2rx7*$^{fl/fl}$ mice (Fig. 2Q).

Together, these data demonstrate a cell type-specific contribution of the P2X7R to the generation of seizures. Loss of neuronally-expressed P2X7R renders mice more susceptible to seizures, whereas the loss of P2X7R in microglia reduces the seizure threshold.

3.3. P2X7R deficiency in microglia promotes an anti-inflammatory microglia phenotype following SE

We next wanted to explore the effects the deletion of the P2X7R has on different cell types during seizures focusing first on microglia. Analysis of gene expression in hippocampal samples from *P2rx7*$^{-/-}$-M compared to *P2rx7*$^{fl/fl}$ mice revealed no baseline differences in microglia activation markers. In contrast, there was enhanced expression of anti-inflammatory genes (*Mrc1* (*Cd206*), *Arg1*, *p2ry12*) and lower expression of pro-inflammatory genes (*Cd86*, *Il-6*, *Iba-1*) in *P2rx7*$^{-/-}$-M mice when compared to IAKA-injected *P2rx7*$^{fl/fl}$ mice (Fig. 3A, B). This suggests that the P2X7R in microglia contributes to pro-inflammatory responses during SE. No changes in microglia-specific genes were observed when comparing gene profiles from tamoxifen-treated Cre mice with *P2rx7*$^{fl/fl}$ mice, confirming these changes are due to the deletion of P2X7Rs on microglia and not a non-specific effect of the expression of Cre (Supplementary Fig. 6A). Further suggesting effects are specific to microglial P2X7Rs, no changes in microglial genes were

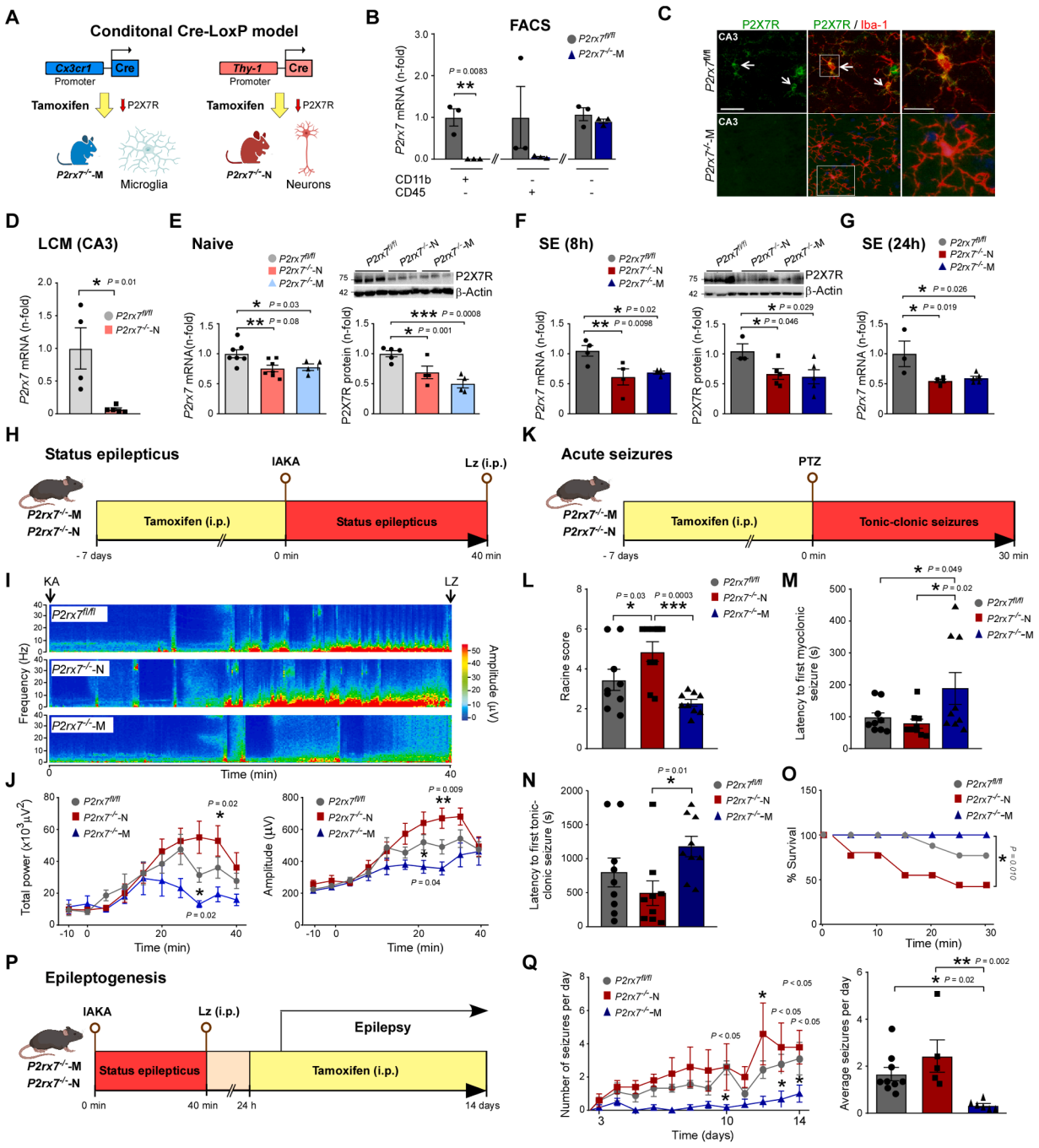

Fig. 2. Cell type-specific effects of P2X7Rs on seizures. (A) Cell type-specific approach to achieve a conditional cell type-specific knockdown of P2X7R in microglia (*P2rx7*$^{-/-}$-M) and neurons (*P2rx7*$^{-/-}$-N). (B) *P2rx7* mRNA levels in FACS-separated hippocampal microglia and macrophages from tamoxifen-treated *P2rx7*$^{fl/fl}$ and *P2rx7*$^{-/-}$-M mice 40 min post-IAKA ($n = 3$ per group). (C) Co-localization (arrows) of P2X7R (green) with Iba-1 (red) in the hippocampus (CA3 region) of *P2rx7*$^{-/-}$-M mice 40 min post-IAKA post-tamoxifen treatment. Scale bar = 20 μm and 10 μm for magnification. (D) *P2rx7* mRNA levels in the CA3 subfield post-tamoxifen-treatment ($n = 4$ (*P2rx7*$^{fl/fl}$), 5 (*P2rx7*$^{-/-}$-N)). (E) Hippocampal *P2rx7* mRNA and protein levels post-tamoxifen treatment (mRNA: $n = 7$ (*P2rx7*$^{fl/fl}$), 7 (*P2rx7*$^{-/-}$-N), 4 (*P2rx7*$^{-/-}$-M); protein: $n = 5$ (*P2rx7*$^{fl/fl}$), 4 (*P2rx7*$^{-/-}$-N), 4 (*P2rx7*$^{-/-}$-M)) in naïve conditions and (F) 8 h post-IAKA (mRNA: $n = 4$ (*P2rx7*$^{fl/fl}$), 4 (*P2rx7*$^{-/-}$-N), 4 (*P2rx7*$^{-/-}$-M)); protein: $n = 3$ (*P2rx7*$^{fl/fl}$), 5 (*P2rx7*$^{-/-}$-N), 5 (*P2rx7*$^{-/-}$-M)). (G) *P2rx7* mRNA levels in the ipsilateral hippocampus 24 h post-IAKA-induced SE of mice with a knockdown in microglia (*P2rx7*$^{-/-}$-M) and neurons (*P2rx7*$^{-/-}$-N) when compared to *P2rx7*$^{fl/fl}$ mice ($n = 3$ *P2rx7*$^{fl/fl}$, 4 *P2rx7*$^{-/-}$-N, 5 *P2rx7*$^{-/-}$-M). (H) Experimental approach to study impact of cell type-specific P2X7R knockdown on IAKA-induced SE. (I) Representative EEG heat maps during IAKA-induced SE. (J) EEG total power and amplitude from IAKA until lorazepam ($n = 18$ (*P2rx7*$^{fl/fl}$), 14 (*P2rx7*$^{-/-}$-N), 13 (*P2rx7*$^{-/-}$-M)). (K) Experimental approach to study impact of cell type-specific P2X7R knockdown on PTZ-induced seizures. (L) Behavior seizures of tamoxifen-treated *P2rx7*$^{fl/fl}$, *P2rx7*$^{-/-}$-N and *P2rx7*$^{-/-}$-M mice post-PTZ ($n = 9$ per group). (M) Threshold to first myoclonic and (N) tonic-clonic seizure in tamoxifen-treated *P2rx7*$^{fl/fl}$, *P2rx7*$^{-/-}$-N and *P2rx7*$^{-/-}$-M mice post-PTZ ($n = 9$ per group). (O) Survival analysis of tamoxifen-treated *P2rx7*$^{fl/fl}$, *P2rx7*$^{-/-}$-N and *P2rx7*$^{-/-}$-M mice for the first 30 min post-PTZ ($n = 9$ per group). (P) Design to study impact of cell type-specific P2X7R knockdown on epilepsy. (Q) Daily seizure counts in tamoxifen-treated IAKA subjected mice until day 14 post-SE ($n = 9$ (*P2rx7*$^{fl/fl}$), 5 (*P2rx7*$^{-/-}$-N), 6 (*P2rx7*$^{-/-}$-M)). E, F, G, L, M, N, Q (right graph), One-way ANOVA with Fischer's multiple-comparison test. B, D, Unpaired Student's *t*-test. J, Q (left graph), Two-way ANOVA with Tukey's multiple comparisons test. O, Log-rank (Mantel-Cox) test. Data are shown as mean ± SEM. $^{*}P < 0.05$; $^{**}P < 0.01$; $^{***}P < 0.001$. Created with BioRender.com. (For interpretation of the references to color in this figure legend, the reader is referred to the web version of this article.)

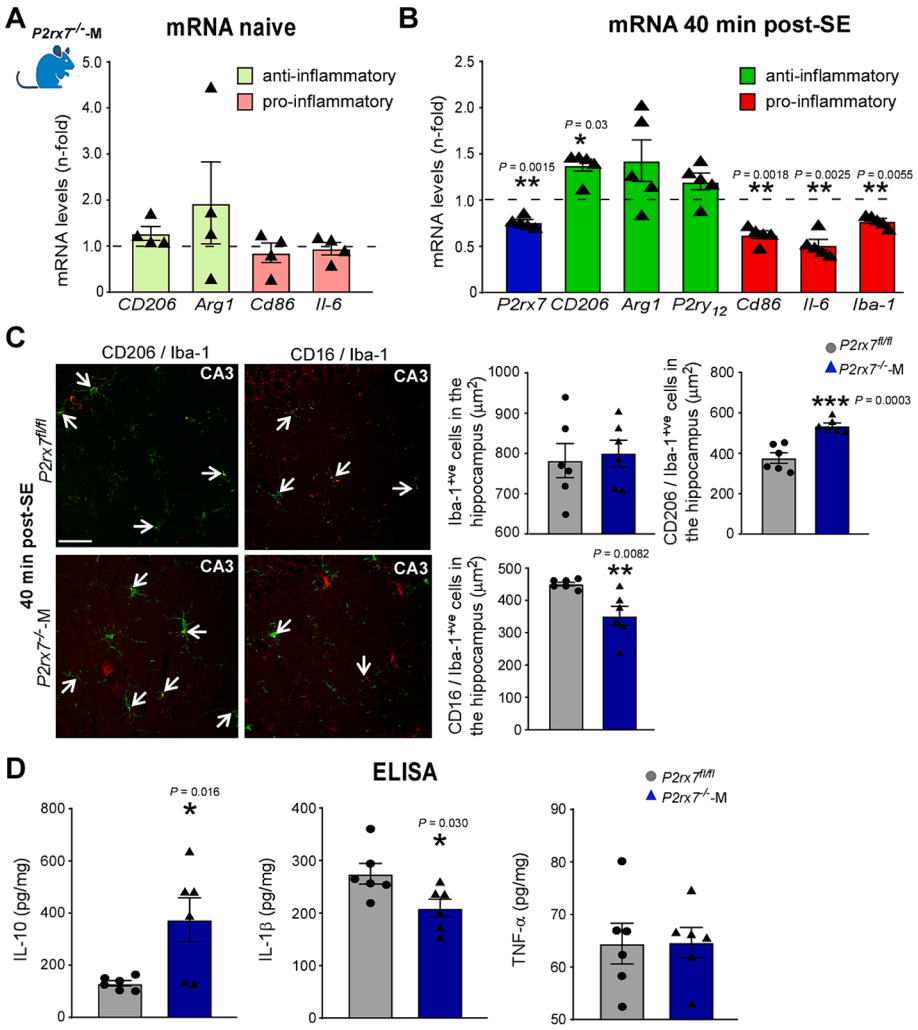

Fig. 3. P2X7R deficiency in microglia promotes an anti-inflammatory microglia phenotype post-SE. (A) Hippocampal mRNA levels of the anti-inflammatory markers *Cd206* and *Arg1* and pro-inflammatory markers *Cd86* and *Il-6* of tamoxifen-treated *P2rx7*$^{-/-}$-M mice compared to control *P2rx7*$^{fl/fl}$ mice (n = 4 per group). (B) Hippocampal (ipsilateral) mRNA levels of the anti-inflammatory marker *Cd206*, and pro-inflammatory markers *Cd86, Il-6* and *Iba-1* in tamoxifen- *P2rx7*$^{-/-}$-M mice 40 min post-IAKA compared to tamoxifen-treated treated *P2rx7*$^{fl/fl}$ subjected to IAKA (n = 5 per group). (C) Degree of co-localization of CD206 (red) or CD16 (red) with microglia marker Iba-1 (green) in the ipsilateral hippocampus (CA3 region) of tamoxifen-treated *P2rx7*$^{fl/fl}$ and *P2rx7*$^{-/-}$-M mice 40 min post-IAKA. White arrows indicate co-localization (n = 6 per group). Scale bar = 50 µm (D) IL-10, IL-1β and TNF-α levels in the ipsilateral hippocampus of tamoxifen-treated *P2rx7*$^{fl/fl}$ and *P2rx7*$^{-/-}$-M mice 40 min post-IAKA (n = 6 per group). A, B, One-way ANOVA with Fischer's multiple-comparison test. C, D, Unpaired Student's t-test. Data are shown as mean ± SEM. *$P < 0.05$; **$P < 0.01$; ***$P < 0.001$. Created with BioRender.com. (For interpretation of the references to color in this figure legend, the reader is referred to the web version of this article.)

observed in *P2rx7*$^{-/-}$-N mice post-SE (Supplementary Fig. 6B). To extend these findings, we performed double staining for the microglia marker Iba-1 and the anti-inflammatory microglia marker CD206. This showed an elevated number of CD206-positive cells in the hippocampus of *P2rx7*$^{-/-}$-M mice post-IAKA (Fig. 3C). In contrast, there were a reduced number of CD16-positive cells, a pro-inflammatory marker, in the hippocampus of *P2rx7*$^{-/-}$-M mice after SE. While no obvious changes in microglia morphology between genotypes could be observed post-SE, microglia in *P2rx7*$^{-/-}$-M mice showed slightly longer primary processes (Supplementary Fig. 7), suggestive of a more anti-inflammatory phenotype (Leyh, 2021). ELISA analysis of hippocampal tissue obtained 40 min post-IAKA showed higher levels of the anti-inflammatory cytokine IL-10 and lower levels of the pro-inflammatory cytokine IL-1β in *P2rx7*$^{-/-}$-M mice when compared to *P2rx7*$^{fl/fl}$ mice. No change in TNF-α levels was observed between genotypes (Fig. 3D).

3.4. Increased neuronal P2X7R expression in the brain of TLE patients

The increased seizure severity observed in *P2rx7*$^{-/-}$-N mice suggests a functional role of the P2X7R in neurons. P2X7R protein expression has been reported in neurons in rodent models of epilepsy, but this remains contested (Beamer, 2021; Kaczmarek-Hajek, 2018). To determine if neurons express the P2X7R in the human brain, we analysed a single-nuclei RNA sequencing dataset from the neocortex of TLE patients and controls (Pfisterer, 2020). Due to the NeuN-based nuclei sorting used, glia subtype data were not available for comparison. Using validated markers of the major neuron subtypes, we detected the expression of *P2RX7* in both principal excitatory neurons and GABAergic interneuron subtypes (Fig. 4A). Notably, *P2RX7* expression was detected in a higher proportion of cells (20–50 % of principal neurons, and 10–20 % of GABAergic interneurons) when compared to the six other P2XR family members (Fig. 4B). We also performed differential expression analysis, and identified that *P2RX7* expression was significantly up-regulated in epilepsy samples in both principal and GABAergic interneuron subtypes, compared to controls (Fig. 4C). Interestingly, *P2RX4* was the only other P2XR gene showing altered expression in human TLE, with its expression increased in principal neuron subpopulations but not GABAergic interneurons (Fig. 4C). We also noted that the level of *P2RX7* RNA

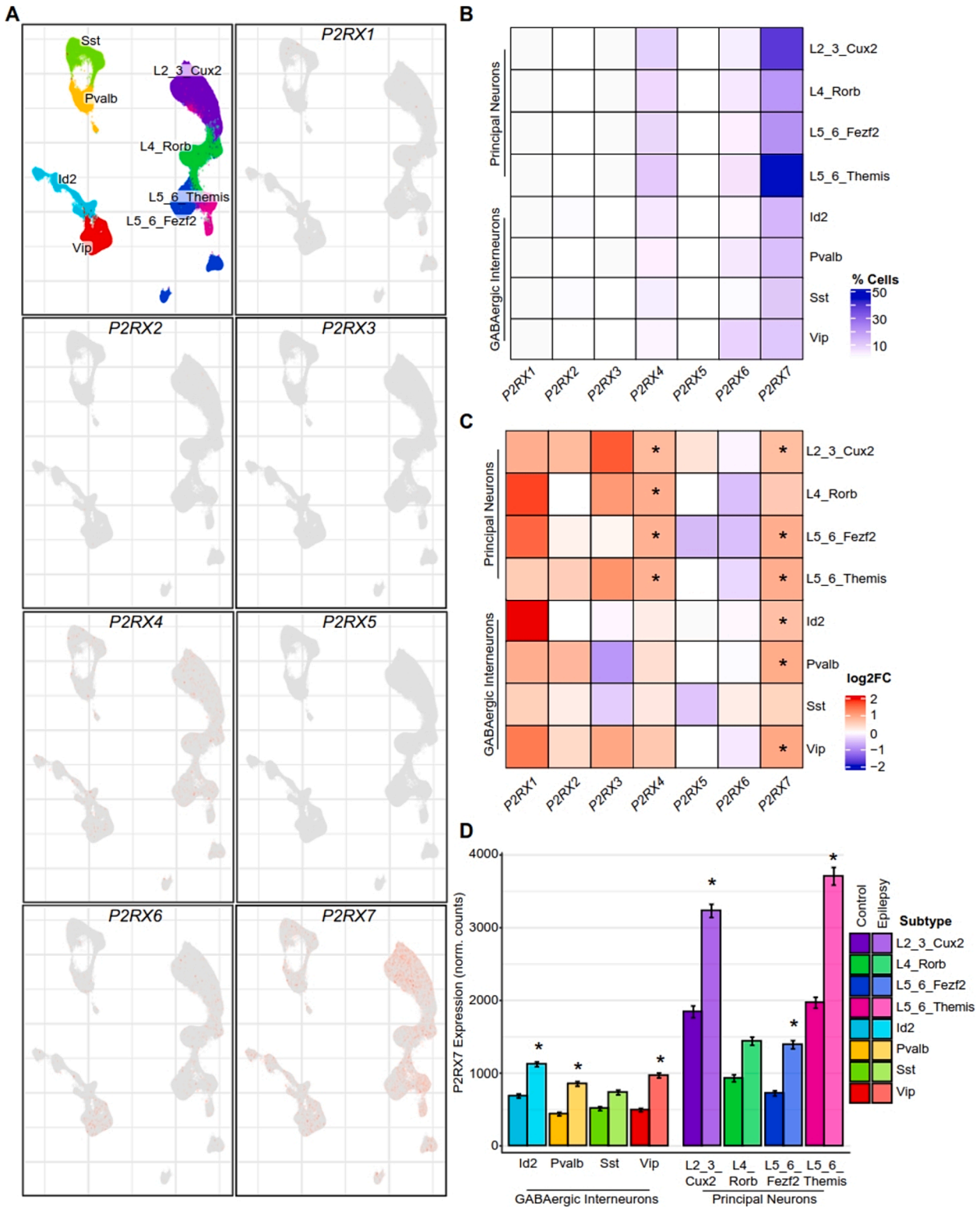

Fig. 4. P2RX family expression and dysregulation in human TLE and control samples. (A) Uniform Manifold Approximation and Projection (UMAP) representation of single nuclei from human TLE and control temporal cortex samples. The coloured clusters in the first panel represent 8 neuronal subtypes as defined by expression of key subtype markers (Figure adapted from Fig. 1C in *Pfisterer et al.*, 2020). Red/grey colour scale is "proportional to log-normalised expression values" across single cells. (B) Percentage of cells in each neuronal subtype in which expression of P2RX family members was detected. (C) Differential expression (log_2 Fold-change) of P2RX family members between human TLE and control samples across the 8 neuronal subtypes. Red shading indicates higher expression of the gene in epilepsy samples, while blue shading indicates lower expression in epilepsy samples. Statistical significance with FDR < 0.05 is marked by *. (D) Expression (mean ± st. dev.) of *P2RX7* in neuronal subtypes from control and epilepsy samples. * FDR < 0.05. (For interpretation of the references to color in this figure legend, the reader is referred to the web version of this article.)

seemed to be lower in GABAergic interneurons when compared to glutamatergic principal neurons (Fig. 4D). These human data confirm that the *P2RX7* transcript is expressed in the major subtypes of human neurons.

3.5. Enhanced P2X7R function on GABAergic interneurons in epilepsy

Our sequencing results in the IAKA model suggest GABAergic interneurons are the neuronal subtype that is mostly affected via P2X7R signaling during seizures. To further explore whether P2X7Rs are functional in these neuronal subtypes during epilepsy, we labelled GABAergic interneurons in the mouse brain by injection of an AAV expressing the green fluorescent protein (GFP) under the distal-less homeobox (mDlx) promoter (GFP-AAV^{Dlx}) (Dimidschstein, 2016) (Fig. 5A). We focused on the hilar region of the hippocampus, because surviving hilar GABAergic interneurons have been reported to become less active in epileptic animals (Sloviter, 2003). Increasing activity of hilar GABAergic interneurons therefore may represent a promising avenue to increase the inhibitory drive in the hippocampus and in turn reduce hyperexcitability (Righes Marafiga et al., 2021).

GFP-labelled cells in the hippocampus, in particular within the hilar region, could be observed two- and three-week post-infection (Supplementary Fig. 8). Accordingly, subsequent experiments were carried out two weeks post-AAV transduction. Counter-staining of GFP-positive cells with antibodies against parvalbumin confirmed the AAVs had transduced GABAergic interneurons in the hippocampus (Fig. 5B). Next, we carried out GFP-guided patch clamp recordings from GFP-positive cells under control conditions and 14 days post-IAKA (epilepsy was

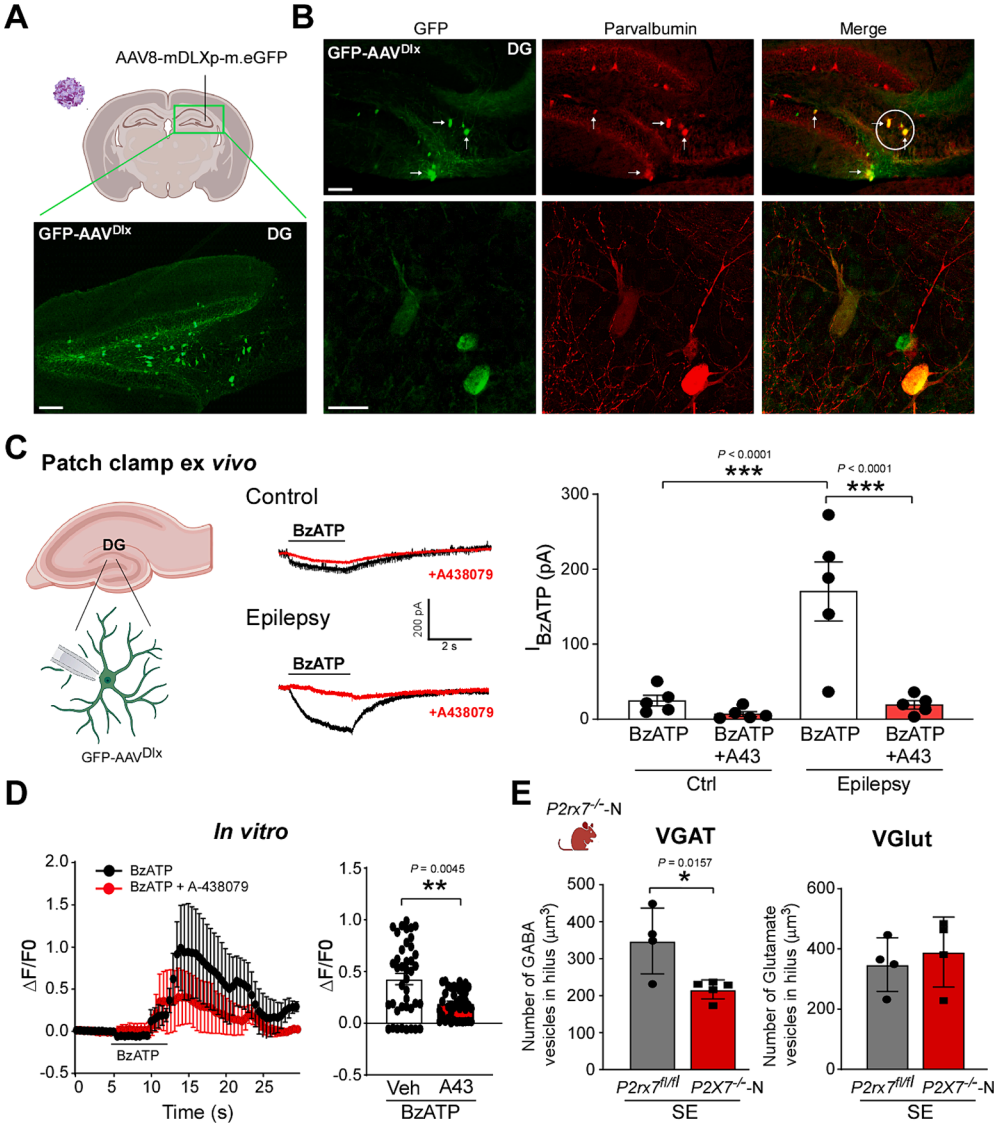

Fig 5. Increased P2X7R function in GABAergic interneurons during epilepsy. (A) Schematic showing injection site for GFP-AAV^{Dlx} delivery and representative image of GFP staining in the hilar region of the dentate gyrus (DG) of mice 2 weeks-post GFP-AAV^{Dlx} transduction (representative image from a total of 3 mice per group). Scale bar = 100 µm. (B) Co-staining against GFP and Parvalbumin in the hilus 2 weeks post-AAV injection (representative images from three mice per group). Scale bar = 50 µm and 10 µm for magnification (C) Representative currents evoked by BzATP (100 µM; 3 s) in GFP-labelled hilar interneurons (control, Crtl) and during epilepsy (*i.e.*, 14 days post-SE) in the absence (black trace) and presence of A-438079 (10 µM) (red trace). Vh = -70 mV. Graph shows peak amplitude of BzATP-induced currents in GFP-positive cells (n = 5 cells per group; cells were recorded from 2 Control mice and one epileptic mouse)). (D) Graph showing quantified ΔF/F0 values for a duration of 20 s upon BzATP application in the absence or presence of A-438079 (10 µM) (n = 42 measurements per group were taken from 3 cells). (E) VGAT-and VGLUT-positive vesicle numbers in the ipsilateral hilus of *P2rx7*$^{fl/fl}$ and *P2rx7*$^{-/-}$-N mice post-IAKA-induced SE (n = 4 (*P2rx7*$^{fl/fl}$), 5 (*P2rx7*$^{-/-}$-N)). C, One-way ANOVA followed by Fischer's multiple-comparison test. D, Mann–Whitney U test. E, Unpaired Student's t-test. $^{**}P < 0.01$; $^{***}P < 0.001$. .Created with BioRender.com. (For interpretation of the references to color in this figure legend, the reader is referred to the web version of this article.)

confirmed via behavioral seizures) (Fig. 5C). In control mice, the P2X7R agonist BzATP (3′-O-(4-Benzoyl)benzoyl ATP) evoked small currents in GABAergic interneurons which were not significantly decreased by co-incubation with the P2X7R antagonist A438079 (Fig. 5C). In contrast, BzATP-evoked currents were approximately 4-fold greater in GFP-positive neurons during epilepsy and could be blocked by the P2X7R antagonist A438079, confirming they were primarily mediated by the P2X7R (Fig. 5C). These findings were extended by *in vitro* recordings of functional P2X7R expression on GABAergic interneurons. Specifically, BzATP application in AAV-transduced mouse primary cell cultures resulted in BzATP-mediated intracellular Ca^{2+} increase, which was partially reduced by A-438079 (Fig. 5D). Further suggesting neuronal P2X7R contributing to the regulation of brain GABA levels, *P2rx7*$^{-/-}$-N mice showed lower GABA levels in the hilus when compared to *P2rx7*$^{fl/fl}$ mice post-SE confirmed via lower abundance of vesicular GABA transporter (VGAT)-positive vesicles in the hilus (Fig. 5E, Supplementary Fig. 9). In contrast, no changes in the number of vesicular glutamate transporter 1 (VGLUT)-positive vesicles in the hilus could be observed between genotypes (Fig. 5E, Supplementary Fig. 9).

3.6. P2X7R overexpression in GABAergic interneurons reduces seizure severity and suppresses epileptic seizures

Based on our findings, we hypothesized that the P2X7R on neurons is

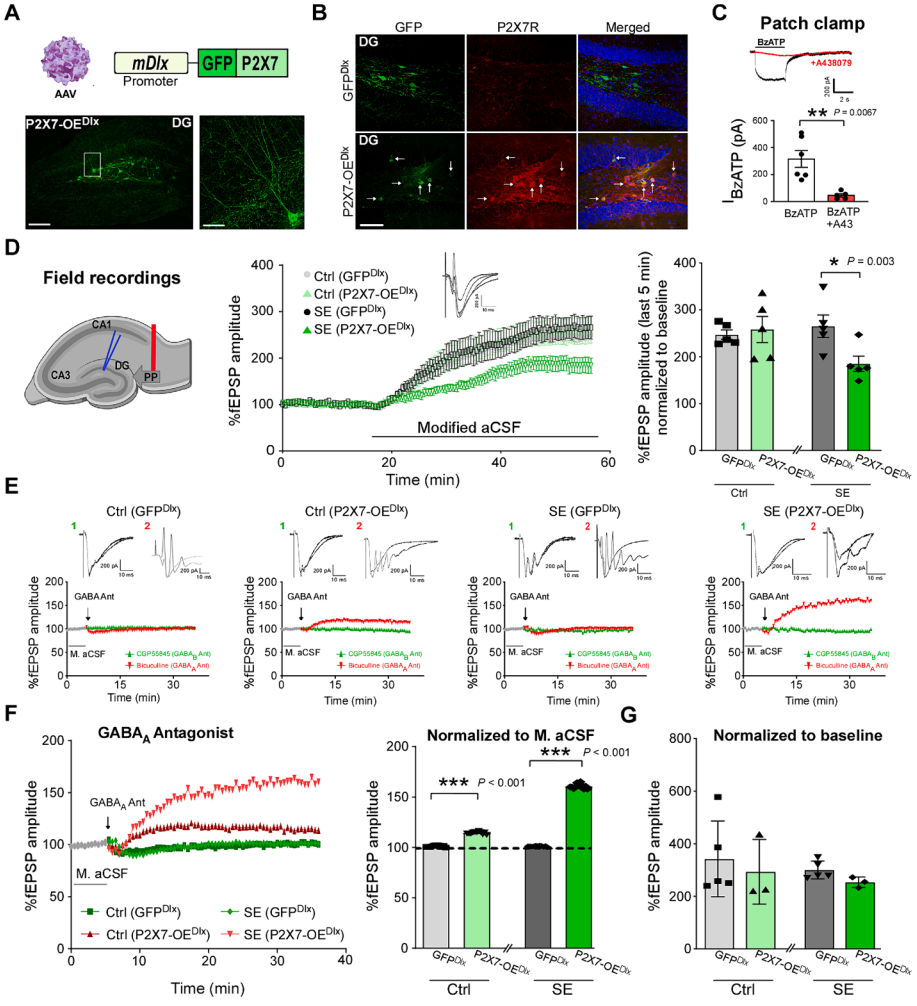

Fig. 6. Decreased brain hyperexcitability via P2X7R overexpression in GABAergic interneurons. (A) P2X7R fused to eGFP was overexpressed via AAV under the mDlx promoter. Transduced cells in the hippocampus 2 weeks post-AAV injection (representative images from a total of 3 mice). Scale bar = 100 μm. (B) Co-staining against GFP (green) and P2X7R (red) in hippocampal tissue sections of GFP-AAV^{DLx}- and P2X7R-AAV^{Dlx}-transduced mice 2 weeks post-AAV injection and 40 min post-IAKA (representative images from a total of 3 mice). Scale bar = 50 μm. (C) Representative currents evoked by BzATP (100 μM; 3 s) in GFP-labelled hilar interneurons from mice transduced with P2X7R-AAV^{Dlx} in the absence (black trace) and the presence of A-438079 (10 μM) (red trace). Vh = -70 mV. Measurements were carried out 2 weeks post-IAKA. Graph shows peak amplitude of BzATP-induced currents with and without A-438070 ($n = 6$ (BzATP) and 5 (BzATP + A-438070 from 2 mice). (D) Schematic of electrode placement. A stimulating electrode (red) and an extracellular borosilicate glass recording electrode (blue), filled with recording/normal aCSF (R. aCSF), were placed in the perforant pathway (PP) of the DG. fEPSPs were recorded and the amplitude of the signal was measured for 20 min to establish base line. Exposure to M. aCSF (modified Mg^{2+} -free aCSF) for 40 min was used to induce hyperexcitability. Traces represent %fEPSP amplitude normalized to the average value of the last 5 min of baseline. Representative signals from P2X7-OE^{Dlx} and GFP^{Dlx} mice after 40 min of SE, or in control conditions, are displayed ($n = 7$ (GFP^{Dlx}) and 5 (P2X7-OE^{Dlx})). (E) Representative traces of the effects of GABA antagonists on levels of hyperexcitability. CGP-55845 and Bicuculline were added to circulating M. aCSF for 30 min. Representative signals of fEPSPs before and after addition of CGP-55845 (1) and Bicuculline (2), are displayed. (F) Representative traces and graph showing effects of Bicuculline on levels of synaptic excitability. Traces represent %fEPSP amplitude normalized to the average value of the last 5 min of M. aCSF before drug exposure ($n = 5$ (GFP^{Dlx}) and 3 (P2X7-OE^{Dlx})). (G) fEPSPs of brain slices from P2X7-OE^{Dlx} and GFP^{Dlx} mice after 40 min of SE, or in control conditions, treated with Bicuculline and normalized to average value of the last 5 min of baseline ($n = 5$ (GFP^{Dlx}) and 3 (P2X7-OE^{Dlx})). C, D, F (right graph), Unpaired Student's *t*-test. *$P < 0.05$; **$P < 0.01$; ***$P < 0.001$. Created with BioRender.com. (For interpretation of the references to color in this figure legend, the reader is referred to the web version of this article.)

upregulated during epilepsy and may function to regulate neurotransmitter release and network excitability. Because our results suggest P2X7R-dependent signaling during seizures to impact particularly on the GABAergic signaling system (*e.g.*, high number of GABAergic genes altered in *Prx7*$^{-/-}$ mice and lower abundance of VGAT-positive vesicles in *P2rx7*$^{-/-}$-N mice post-SE), for our next experiments we focused on the role of P2X7R in GABAergic interneurons. Moreover, failures of the GABAergic inhibitory system are widely acknowledged as contributors to seizures, consequently, methods boosting GABAergic signaling in the brain represent plausible therapeutic avenues (Mula, 2011; Magloire, 2019). We speculated that enhancing expression on GABAergic interneurons, which express low levels of the *P2rx7 m*RNA, may increase inhibitory neurotransmission. Accordingly, we adapted the AAVs to express the murine full-length P2X7R isoform linked to the fluorescent reporter protein GFP under the same mDlx promoter (P2X7R-AAV^{Dlx}) as before (Dimidschstein, 2016) to generate P2X7R overexpressing mice (P2X7-OE^{Dlx}) (Fig. 6A). As above, mice received injections of P2X7R-AAV^{Dlx} and, after a two-week delay, brains were analysed for correct expression. Co-staining against GFP and P2X7R confirmed P2X7R overexpression in transduced mice (Fig. 6B). We next used patch clamp recordings from brain slices to confirm that P2X7R-AAV^{Dlx} increased P2X7R function in GABAergic interneurons. BzATP-induced currents measured in GFP-positive cells in epileptic mice (all mice showed behavior seizures confirming epilepsy development) were increased by over 50 % to approximately 300 pA when compared to currents recorded during epilepsy with the empty GFP vector (approximately 180 pA, see Fig. 5C) (Fig. 6C). Thus, we successfully increased the P2X7R component specifically in GABAergic interneurons in mice.

To test whether P2X7R overexpression in GABAergic interneurons reduces hyperexcitability in the hippocampus, brain slices from P2X7R-AAV^{Dlx}-transduced mice (Control and post-SE) were analyzed via field recordings. Epileptiform-like activity was provoked using the well-established low Mg^{2+} model of seizures. Synaptic activity in hippocampal slices was increased by 2.5-fold following exposure to low Mg^{2+} artificial cerebrospinal fluid (aCSF) for 40 min. Slices from epileptic mice previously transduced with P2X7R-AAV^{Dlx}, however, showed a significantly smaller increase, while no difference was observed between the remaining treatment groups (Fig. 6D). These findings suggest that elevating the P2X7R in GABAergic interneurons enhances inhibitory drive only in the context of a pre-existing hyperexcitable state. A possible explanation is that only pathophysiologically increased ATP levels are sufficient to activate the P2X7R.

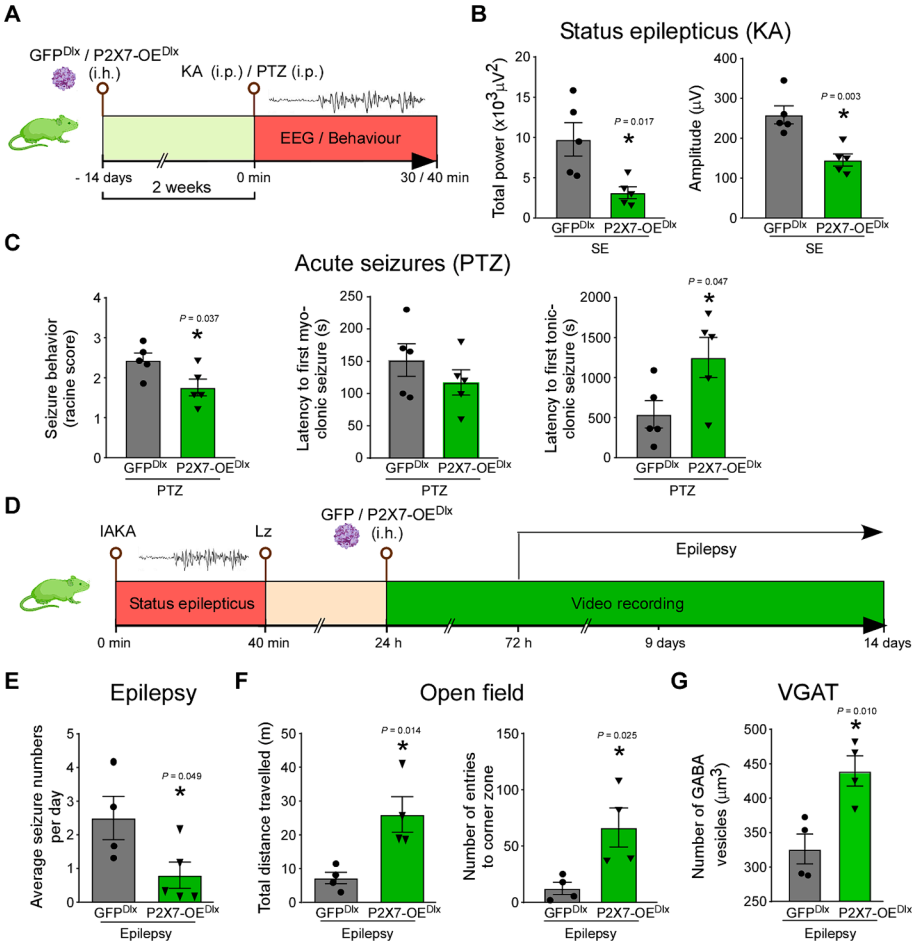

Fig 7. AAV-mediated P2X7R overexpression in GABAergic interneurons reduces acute seizure severity and leads to a milder epilepsy phenotype. (A) Experimental design to test anticonvulsant potential of increased P2X7R overexpression in GABAergic interneurons. Mice were transduced with GFP-AAV^{Dlx} or P2X7R-AAV^{Dlx} 2 weeks prior to treatment with proconvulsant (*i.e.*, i.p. KA or PTZ). (B) EEG total power and amplitude during a 90 min recording period from the time of i.p. KA of GFP^{Dlx} and P2X7-OE^{Dlx} transduced mice subjected to i.p. KA ($n = 5$ per group). (C) Average seizure behavior (Racine score) during 30 min following PTZ injection, latency to first myoclonic seizure and latency to first tonic clonic seizure in mice transduced 2 weeks before with GFP-AAV^{Dlx} (GFP^{Dlx}) and P2X7R-AAV^{Dlx} (P2X7-OE^{Dlx}) ($n = 5$ per group). (D) Experimental design to analyze impact of P2X7R overexpression on epilepsy. AAV was delivered intra-hippocampal (i.h.) after-IAKA injection and mice recorded via video recordings from day 9 to day 14 post-IAKA. (E) Average number of spontaneous seizures per day ($n = 4$ (GFP^{Dlx}) and 5 (P2X7-OE^{Dlx})). (F) Graphs showing total distance travelled and number of entries to the corner zone of epileptic GFP^{Dlx} and P2X7-OE^{Dlx} mice ($n = 4$ per group). (G) VGAT-positive vesicle numbers in the ipsilateral hilus of epileptic GFP^{Dlx} and P2X7-OE^{Dlx} mice ($n = 4$ per group). B, C, E, F, G, Unpaired Student's *t*-test. Data are shown as mean ± SEM. *$P < 0.05$. Created with BioRender.com.

To establish whether the reduced hyperexcitability observed in brain slices from P2X7-OE^{Dlx} mice subjected to IAKA were due to increased GABAergic signaling, brain slices were treated with CGP-55845 hydrochloride (CPG), a specific antagonist of the presynaptic $GABA_B$ receptor, and Bicuculline methochloride, a postsynaptic $GABA_A$ receptor antagonist, 40 min following treatment with modified aCSF. Recordings during the application of modified aCSF were taken as baseline measurements (Fig. 6E). Effects on hyperexcitability of both GABA antagonists were similar in brain slices from mice expressing only GFP under control conditions and post-SE. In contrast, treatment of brain slices from P2X7-OE^{Dlx} mice with Bicuculline showed increased hyperexcitability when compared to brain slices treated with CPG. This was particularly evident in brain slices from mice subjected to SE (Fig. 6E, F). Of note, when normalizing traces to baseline recordings, no difference could be observed between treatment groups, further suggesting that seizure-suppressive effects of P2X7R overexpression are mediated via increased GABA signaling (Fig. 6G).

To test whether increased P2X7R expression impacts the seizure threshold *in vivo*, mice were transduced with GFP-AAV^{Dlx} or P2X7R-AAV^{Dlx} and subjected to intraperitoneal (i.p.) KA-induced SE or PTZ 14 days later (Fig. 7A). We used the i.p. KA model instead of the IAKA model, because mice had already been equipped with a cannula to deliver AAVs. When subjected to i.p. KA-induced SE, P2X7-OE^{Dlx} mice showed a lower total power and amplitude on the EEG when compared to GFP-AAV^{Dlx} transduced control mice (Fig. 7B). P2X7R overexpression, while not altering the latency to the first myoclonic seizure, also increased the latency to more severe tonic-clonic seizures in the i.p. PTZ model (Fig. 7C).

To test whether P2X7R overexpression impacts on the epileptic phenotype, mice were subjected to IAKA-induced SE prior to the injection with GFP-AAV^{Dlx} or P2X7R-AAV^{Dlx} (Fig. 7D). While GFP-AAV^{Dlx}-transduced mice experienced an average of approximately 2–3 seizures per day, similar to what has been reported previously for the IAKA model (Jimenez-Mateos, 2012), mice transduced with P2X7R-AAV^{Dlx} experienced fewer seizures per day averaging approximately one seizure per day (Fig. 7E). P2X7-OE^{Dlx} mice also showed less anxiety as evidenced by more entries to the corner zone in the open field (Fig. 7F). NeuN staining confirmed no obvious neurodegeneration in epileptic mice transduced with P2X7-AAV^{Dlx}. In addition, P2X7-OE^{Dlx} mice had similar numbers of GFP-positive interneurons when compared to epileptic mice transduced with GFP-AAV^{Dlx}. No obvious differences in normal behavior were observed between mice transduced with GFP-AAV^{Dlx} or P2X7R-AAV^{Dlx} two weeks post-virus injection as measured in the Open Field (Supplementary Fig. 10A-C). While P2X7-AAV^{Dlx}-transduced epileptic mice showed higher GABA levels in the hippocampus when compared to epileptic GFP-AAV^{Dlx} mice (Fig. 7G), no difference in GABA levels could be observed when comparing non-epileptic GPF-AAV^{Dlx} mice with mice transduced with P2X7R-AAV^{Dlx} (327.3 ± 18.3 vesicles/μm^3 (GFP-AAV) vs 309.9 ± 67.9 vesicles/μm^3 (P2X7-AAV^{Dlx} (n = 2)), suggesting effects of overexpressing P2X7R being restricted to disease conditions and silent during normal physiology.

Finally, to determine whether the seizure-suppressive effects via GABAergic P2X7R overexpression are unique to acquired models of epilepsy that phenocopy human TLE, we took advantage of a mouse model of a genetic epilepsy (Fig. 8A). Dravet syndrome is a rare, severe form of developmental epileptic encephalopathy caused mainly by *de novo* mutations in the *SCN1A* gene. Patients usually present with febrile seizures early during the disease. These then progress to refractory spontaneous seizures and the development of an epileptic encephalopathy (Dravet, 2011). Since the sensitivity to prolonged febrile seizures in Dravet syndrome emerges from the deficiency of GABAergic signaling (Bender, 2012), we investigated whether the overexpression of P2X7R in

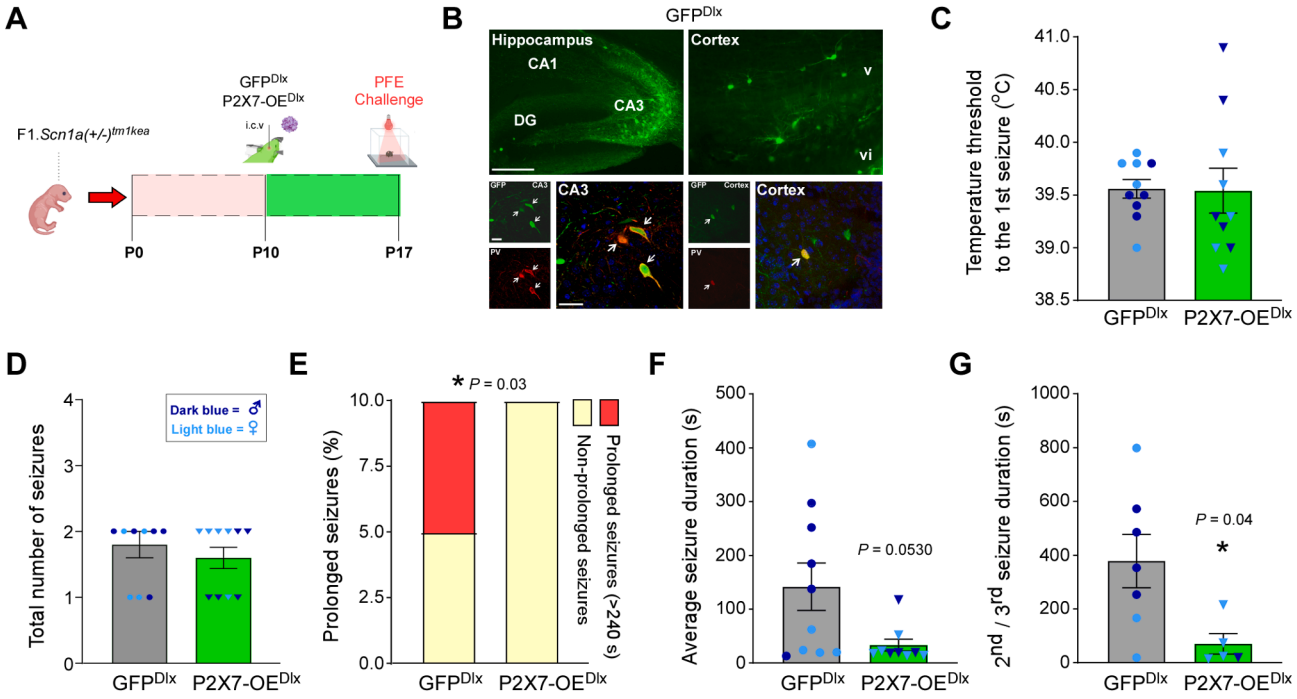

Fig. 8. AAV-mediated P2X7R overexpression in GABAergic interneurons prevents the development of prolonged febrile seizures in a mouse model of Dravet syndrome. (A) At P10, F1.*Scn1a*(+/-)^{tm1Kea} mice were intracerebroventricular (i.c.v.) injected with GFP-AVV^{Dlx} or P2X7R-AAV^{Dlx} to be later submitted to the prolonged febrile event challenge at P17. (B) Representative image of GFP staining in the hippocampus and cortex (layer vi to v) of mice 10 days post GFP-AAV^{Dlx} transduction at P10 (representative image from a total of 3 mice) and co-staining against GFP and parvalbumin. Scale bar = 100 μm and 10 μm for magnification. Graphs show (C) the temperature threshold for mice to develop the first seizure (mild), (D) total number of seizures, (E) percentage of prolonged febrile seizures (F) average seizure duration, and (G) duration of second/third seizure for those animals that experienced more than 1 seizure. One outlier from P2X7-OE^{Dlx} group was removed from the duration of second/third seizure and average seizure duration analyses according to the Grubbs' test (α = 0.0001). (C, D, E: n = 10 per group (5 males and 5 females); F: n = 7 GFP-AVV^{Dlx} (4 males and 3 females) and 5 P2X7R-AAV^{Dlx} (1 male and 4 females)). C, D, F, G Mann-Whitney test. E, Fisher's exact test. Data are shown as mean ± SEM *P < 0.05. Created with BioRender.com.

GABAergic interneurons could prevent the development of prolonged febrile seizures in F1.*Scn1a*$(+/-)^{tm1kea}$ mice when subjected to the prolonged febrile event (PFE) challenge. Analysis of brain tissue 10 days post-GFP-AAV^{Dlx} injection at day P10 confirmed GFP-positive neurons in several brain structures including the hippocampus, cortex and thalamus (Fig. 8B and Supplementary Fig. 11)). Of note, similar to adult mice, double staining with parvalbumin confirmed transduction of GABAergic interneurons (Fig. 8B). While the temperature was raised and held at 41 °C, F1.*Scn1a*$(+/-)^{tm1kea}$ mice from both treatment groups experienced a similar temperature threshold to develop the first mild seizure and number of seizures (Fig. 8C, D). In contrast, 50 % of F1. *Scn1a*$(+/-)^{tm1Kea}$ control mice developed prolonged seizures (>240 s) which was completely prevented by the transduction of P2X7R-AAV^{Dlx} in F1.*Scn1a*$(+/-)^{tm1Kea}$ mice (Fig. 8E, F). P2X7R-AAV^{Dlx} transduced F1. *Scn1a*$(+/-)^{tm1Kea}$ mice also showed ~ 90 % reduction in the duration of the 2nd/3rd seizure (Fig. 8G), similarly to our findings observed in the PTZ model.

4. Discussion

Here, we show cell type-dependent divergent effects of the P2X7R in the regulation of brain hyperexcitability in the setting of epilepsy. We show that loss of the P2X7R from microglia has anti-convulsive and anti-epileptogenic effects, whereas its deletion from neurons increases excitability and leads to a more severe seizure phenotype. We also demonstrate that the P2X7R is functional during epilepsy in inhibitory interneurons in the brain and show that overexpression of P2X7R in GABAergic interneurons reduces seizures in acquired and genetic models of epilepsy. Together, our findings may explain previous conflicting findings on the seizure-modifying actions of the P2X7R and indicate P2X7R-based precision and gene therapy approaches to enhance inhibitory neuron function to treat epilepsies.

A key result of the present study was that microglial P2X7R indeed drives inflammatory signaling and contributes to hyperexcitability. This is based on the finding that mice lacking the receptor in microglia show less severe seizures during IAKA-induced SE and following PTZ treatment and develop a milder epileptic phenotype. These results are in line with inflammation contributing to brain hyperexcitability and drugs blocking neuroinflammation increasing the seizure threshold (Vezzani et al., 2019). The P2X7R has been described as a key driver of inflammation contributing to the activation of the NLRP3 inflammasome and the proliferation and activation of microglia (Monif, 2009; Campagno and Mitchell, 2021; Pelegrin, 2021). Previous studies have shown P2X7R antagonism to reduce IL-1β levels in the hippocampus post-SE (Engel, 2012) and to reduce microgliosis and astrogliosis during epilepsy (Jimenez-Pacheco, 2016). More recently, we have shown that increased P2X7R activation post-SE leads to a pro-inflammatory phenotype in microglia (Beamer, 2022), and, conversely, that blocking of the P2X7R leads to an anti-inflammatory microglial phenotype following seizure in a mouse model of neonatal hypoxia induced-seizures (Smith, 2023). Of note, our study shows a strong up-regulation of the cytokine IL-10 and reduction of IL-1β in the hippocampus of mice with a microglia P2X7R deletion. This suggests that the lack of P2X7R in microglia during seizures promotes a neuroprotective microglia phenotype, increasing the release of anti-inflammatory mediators and, at the same time, decreasing pro-inflammatory signaling. The pro-convulsant function of IL-1β is well-established (Maroso, 2010) and IL-10 is a known anti-epileptic cytokine. Interestingly, recent data show that IL-10 enhances GABAergic signaling which is antagonized by IL-1β (Ruffolo, 2022). IL-10 has, however, also been shown to reduce IL-1β levels (Ruffolo, 2022). While our results suggest that the pro-convulsant effects of P2X7R on microglia are mediated via P2X7R promoting a pro-inflammatory phenotype in microglia, thereby, increasing the pro-inflammatory tissue tone, we cannot exclude other effects contributing to seizures and epilepsy. The P2X7R has been shown to regulate numerous pathways in microglia (*e.g.*, clearance of extracellular and intracellular debris) (Campagno and Mitchell, 2021), which contribute to seizures and epilepsy (Kinoshita and Koyama, 2021). Of note, while microglia had previously been ascribed a mainly pro-convulsant role, data also suggests a protective function of microglia, with the depletion of microglia leading to a more severe seizure phenotype (Badimon, 2020; Liu, 2020). This suggests that the targeting of specific pathways (*e.g.*, P2X7R) is most likely more effective than blocking microglia function as a whole.

The present study further sheds light on a long-standing debate in the field around whether or not neurons express functional P2X7Rs. We show that human neurons express *P2RX7* mRNA and indeed at higher levels than other P2RX family members, and that *P2RX7* expression is increased in long-standing epilepsy. Importantly, in our epilepsy mouse model, these receptors become functional on inhibitory neurons. Consistent with an attenuation of excitability by P2X7R expression, its neuron-specific deletion exacerbated seizure severity during SE and neuronal damage and led to reduced GABA levels in the brain. This suggests that neuronally-located P2X7Rs control network excitability. Whether these effects are due to P2X7Rs expressed on GABAergic interneurons and/or glutamatergic excitatory neurons, and whether P2X7Rs have a role in neurons under healthy conditions remains to be fully established. We show, however, that human *P2RX7* mRNA levels are increased in both excitatory glutamatergic and inhibitory GABAergic neurons during human TLE, suggesting that P2X7Rs are functional in both neuronal subtypes. Regarding GABAergic interneurons, we further show that P2X7R currents, although hardly detectable under physiological conditions, increase on this neuronal subtype during epilepsy in mice. Thus, we speculate that P2X7R expression on GABAergic interneurons is a useful adaptation and is activated once pathological changes are elicited (*e.g.*, following a seizure or during epilepsy).

Another major finding in the present study was that we could boost inhibition in the brain by overexpressing P2X7R selectively on inhibitory neurons. This worked in both acquired and genetic models, indicating broad relevance to the epilepsies. However, we noticed that the observed effect increases with time. This likely indicates a need for build-up of its ambient agonist, ATP, which happens as seizures continue. Importantly, no obvious neurodegeneration or changes in normal behavior were observed, and neurons transduced with P2X7R-AAV^{Dlx} seemed to be in a healthy state (even in epileptic mice), which would be in contrast to a mainly apoptotic role of P2X7Rs on neurons (Miras-Portugal, 2017). Regarding a possible mechanism of how P2X7R in interneurons suppresses seizures, we have shown GABA-dependence of the seizure-suppressive effects of interneuronal P2X7R in brain slices and increased GABA in the brain of epileptic mice transduced with P2X7R-AAV^{Dlx}. This would be in line with previous evidence showing that P2X7Rs contribute to the release of glutamate and GABA (Papp et al., 2004; Barros-Barbosa, 2018). One could, therefore, hypothesize that increased P2X7R function on interneurons leads to an increase in intracellular Ca^{2+} concentrations, thereby promoting the release of GABA and dampening neuronal hyperexcitability. Interestingly, previous studies have suggested P2X7R to reduce brain hyperexcitability via pre-synaptic inhibition in mossy fibers (Armstrong, 2002). Notably, deficiency in GABAergic signaling is a shared characteristic among numerous brain diseases including depression, mood disorders and several neurodevelopmental disorders (Kim and Yoon, 2017). Thus, increasing GABA signaling via P2X7R overexpression may have more widespread applications beyond epilepsy.

Extracellular ATP is a known damage-associated molecular pattern (DAMP) (Di Virgilio et al., 2020). While ATP is believed to exert a mainly pro-convulsant function, in particular via activation of P2X7Rs in microglia, we here propose that ATP can have both roles, apart from its known role as a source of extracellular adenosine (Dale and Frenguelli, 2009), depending on what cell types are targeted. Under this scenario, upregulated neuronal P2X7Rs would act as a defense mechanism maintaining normal brain hyperexcitability via re-establishing the glutamate/GABA balance in the brain. Once, however, inflammatory

pathways are activated and P2X7R signaling increases on microglia, P2X7R activation leads to the release of pro-inflammatory mediators driving seizures and epilepsy development. Interestingly, we did not observe a clear effect of IAKA in P2X7R KO mice. This may be due to concurrent anticonvulsive (*i.e.,* neurons) and proconvulsive (*i.e.,* microglia) effects that counteract each other. However, once inflammatory processes are ongoing (*e.g.*, late phases of SE, epilepsy), P2X7R-driven pro-convulsant effects may outweigh P2X7R-mediated anticonvulsant effects, hence P2X7R antagonism reduces seizures/epilepsy (Jimenez-Pacheco, 2016; Beamer, 2022; Engel, 2012). The observed cell type-specific effect may also explain the opposing findings in different seizure models where both pro- and anti-convulsive effects of P2X7R antagonism have been reported (*e.g.*, pilocarpine vs IAKA models) (Beamer, 2021).

It is, however, important to keep in mind that, while representing an invaluable tool to examine cell type-specific contributions of target genes to diseases, both *Cx3cr1* and *Thy-1* have been shown to target additional cell types such as macrophages and T-cells which infiltrate the brain during epilepsy, possibly due to a leaky BBB (Bradley et al., 2009; Varvel, 2016; Zhao, 2019; Yue, 2022). We can, therefore, not rule out that other cell types that show high P2X7R expression (*e.g.*, oligodendrocytes (Kaczmarek-Hajek, 2018), contribute to the observed phenotypes. While our experiments using LCM suggests a knock-down of *P2rx7* in CA3 neurons, and while there is a large body of evidence showing the *Thy-1*-Cre promoter to be active on both excitatory and inhibitory neurons (Nosten-Bertrand, 1996; Chen, 2012; Caccavano, 2020; Arime, 2024), whether our *Thy-1*-Cre line (*P2rx7*$^{-/-}$-N mice) leads to *P2rx7* knock-out in both inhibitory and excitatory neurons should be established in future studies. Moreover, non-neuronal mRNA (*e.g.*, from microglia) may have been included in our analysis via LCM, possibly contributing to differences observed in *P2rx7* mRNA levels among genotypes. Lorazepam, which is a $GABA_A$ receptor potentiating drug, was used in some of the present experiments to improve morbidity and reduce mortality. This is unlikely to be a confounder, however, since effects of a cell type-specific P2X7R KO were evident in the intra-amygdala model studies before the administration of the drug and lorazepam was not used in several other studies (*e.g.*, those with PTZ, systemic KA). For our human studies, we have evaluated changes in P2X7R expression via the analysis of single-cell sequencing restricting our analysis to *P2RX7* transcript expression levels. This should be replicated by using P2X7R antibodies to confirm increases in P2X7R expression at the protein level. We have, however, shown increased responses to the P2X7R agonist BzATP in mouse brain slices during epilepsy, suggesting functional P2X7R expression on these neuronal cell types. For our study we have used male mice and potential sex differences of the described P2X7R functions need to be addressed. We have, however, previously shown that both male and female mice with an altered P2X7R expression respond similarly to IAKA (Beamer, 2022).

5. Conclusions

In conclusion, our data demonstrate for the first time a cell type-specific contribution of the P2X7R to seizures and epilepsy and identify upregulation of neuronal P2X7R as an innate defense mechanism protecting the brain from pathological brain hyperexcitability which can in turn be used for new therapeutic approaches.

Funding

This work was supported by funding from Science Foundation Ireland (17/CDA/4708, SFI Centre for Research Training in Genomics Data Science under Grant number 18/CRT/6214 and co-funded under the European Regional Development Fund and by FutureNeuro industry partners 16/RC/3948, 18/RI/5792, 21/RC/10294_P2); from the H2020 Marie Skłodowska-Curie Actions Individual Fellowship (796600), from Irish Research Council Postdoctoral Fellowships (GOIPD/2020/806 and GOIPD/2020/865) from the European Union's Horizon 2020 research and innovation programme under the Marie Sklodowska-Curie grant agreement (No. 766124), the Agencia Estatal de Investigación (Spain) PID2021-127924NB-I00 (funded by MCIN/AEI/10.13039/501100011033) and National Natural Science Foundation of China (31970550). Fondazione Cariverona -Bando Ricerca e Sviluppo 2022 -ID52251-2022.0087. Excellence Project 2023-2027 of the Department of Neuroscience, Biomedicine and Movement Sciences of the University of Verona, funded by the Italian Ministry of University and Research.

CRediT authorship contribution statement

Mariana Alves: Writing – review & editing, Methodology, Investigation, Funding acquisition, Formal analysis, Data curation. **Beatriz Gil:** Writing – review & editing, Investigation, Formal analysis, Data curation. **Javier Villegas-Salmeron:** Investigation, Formal analysis, Data curation. **Valentina Salari:** Methodology, Investigation, Formal analysis, Data curation. **Ricardo Martins-Ferreira:** Writing – review & editing, Investigation, Formal analysis, Data curation. **Marina Arribas Blázquez:** Investigation, Formal analysis, Data curation. **Aida Menéndez Méndez:** Investigation, Formal analysis, Data curation. **Rogerio Da Rosa Gerbatin:** Investigation, Formal analysis, Data curation. **Jonathon Smith:** Investigation, Formal analysis, Data curation. **Laura de Diego-Garcia:** Writing – review & editing, Formal analysis, Data curation. **Giorgia Conte:** Investigation. **Juan Sierra-Marquez:** Investigation, Formal analysis. **Paula Merino Serrais:** Investigation, Formal analysis, Data curation. **Meghma Mitra:** Investigation, Formal analysis. **Ana Fernandez Martin:** Data curation, Formal analysis, Investigation. **Yitao Wang:** Data curation, Formal analysis, Investigation. **Jaideep Kesavan:** Investigation, Formal analysis. **Ciara Melia:** Investigation, Formal analysis. **Alberto Parras:** Investigation, Formal analysis. **Edward Beamer:** Writing – review & editing, Investigation. **Béla Zimmer:** Investigation, Formal analysis. **Mona Heiland:** Methodology. **Brenton Cavanagh:** Data curation, Investigation, Methodology. **Rafael Parcianello Cipolat:** Data curation, Investigation, Methodology. **James Morgan:** Investigation. **Xinchen Teng:** Resources, Supervision, Writing – review & editing. **Jochen H.M. Prehn:** Funding acquisition, Supervision, Writing – review & editing. **Paolo F Fabene:** Writing – review & editing, Supervision. **Giuseppe Bertini:** Writing – review & editing, Supervision. **Antonio R. Artalejo:** Writing – review & editing, Supervision. **Esteban Ballestar:** Writing – review & editing, Formal analysis. **Annette Nicke:** Writing – review & editing, Supervision, Methodology, Investigation. **Luis A. Olivos-Oré:** Writing – review & editing, Investigation, Formal analysis, Data curation. **Niamh M. C. Connolly:** Writing – review & editing, Investigation, Formal analysis. **David C. Henshall:** Writing – review & editing, Funding acquisition. **Tobias Engel:** Writing – review & editing, Writing – original draft, Validation, Supervision, Resources, Project administration, Methodology, Investigation, Funding acquisition, Formal analysis, Data curation, Conceptualization.

Declaration of Competing Interest

The authors declare that they have no known competing financial interests or personal relationships that could have appeared to influence the work reported in this paper.

Data availability

Data will be made available on request.

Acknowledgements

We would like to thank Dr Heiko Düssmann for imaging support and Omiics (Aarhus, Denmark) for RNA sequencing analysis.

Author Contributions

Conceptualization and methodology: M.A., B.G., R.F., N.C., A.N., D. H. and T.E.; Validation, formal analysis, investigation and data curation: M.A., B.G., J.V-S., R.F., M.A-B., A.M-M., J.S., R.R.G., L.D-G., B.C., R.C., G.C., Y.W., A.F., P.M-S., M.M., J.K., C.M., A.P., E.B., B.Z., M.H., L.O-O. and T.E.; Resources: P.M-S., A.A., E.B., A.N., D.H. and T.E.; Writing – original draft preparation: M.A. and T.E.; Writing - review and editing: M.A., R.F., N.C., X.T., J.H.M.P., A.N., D.H. and T.E.; Preparation of Figures: M.A.; B.G., J.V-S., R.F., R.R.G., N.C. and T.E.; Project administration: T.E.; Funding acquisition: M.A., X.T., A.N.,J.H.M.P., D.C.H. and T.E. All authors reviewed the manuscript.

Appendix A. Supplementary data

Supplementary data to this article can be found online at https://doi.org/10.1016/j.bbi.2024.05.023.

References

Alvarez, M.J., et al., 2016. Functional characterization of somatic mutations in cancer using network-based inference of protein activity. Nat Genet 48, 838–847.
Alves, M., et al., 2019. Context-specific switch from anti- to pro-epileptogenic function of the P2Y1 receptor in experimental epilepsy. J. Neurosci. 39 (27), 5377–5392.
Alves, M., Beamer, E., Engel, T., 2018. The metabotropic purinergic P2Y receptor family as novel drug target in epilepsy. Front. Pharmacol. 9, 193.
Alves, M., Smith, J., Engel, T., 2019. Differential expression of the metabotropic P2Y receptor family in the cortex following status epilepticus and neuroprotection via P2Y1 antagonism in mice. Front. Pharmacol. 10, 1558.
Amhaoul, H., et al., 2016. P2X7 receptor antagonism reduces the severity of spontaneous seizures in a chronic model of temporal lobe epilepsy. Neuropharmacology 105, 175–185.
Andrejew, R., et al., 2020. The P2X7 receptor: Central hub of brain diseases. Front. Mol. Neurosci. 13, 124.
Arime, Y., et al., 2024. Activation of prefrontal parvalbumin interneurons ameliorates working memory deficit even under clinically comparable antipsychotic treatment in a mouse model of schizophrenia. Neuropsychopharmacology 49 (4), 720–730.
Armstrong, J.N., et al., 2002. Activation of presynaptic P2X7-like receptors depresses mossy fiber-CA3 synaptic transmission through p38 mitogen-activated protein kinase. J. Neurosci. 22 (14), 5938–5945.
Badimon, A., et al., 2020. Negative feedback control of neuronal activity by microglia. Nature 586 (7829), 417–423.
Barkas, N., et al., 2019. Joint analysis of heterogeneous single-cell RNA-seq dataset collections. Nat. Methods 16 (8), 695–698.
Barros-Barbosa, A.R., et al., 2018. Under stressful conditions activation of the ionotropic P2X7 receptor differentially regulates GABA and glutamate release from nerve terminals of the rat cerebral cortex. Neurochem. Int. 112, 81–95.
Beamer, E., et al., 2021. ATP and adenosine-Two players in the control of seizures and epilepsy development. Prog. Neurobiol. 204, 102105.
Beamer, E., et al., 2022. Increased expression of the ATP-gated P2X7 receptor reduces responsiveness to anti-convulsants during status epilepticus in mice. Br. J. Pharmacol. 179 (12), 2986–3006.
Bender, A.C., et al., 2012. SCN1A mutations in Dravet syndrome: impact of interneuron dysfunction on neural networks and cognitive outcome. Epilepsy Behav. 23 (3), 177–186.
Bernal-Chico, A., et al., 2020. P2x7 receptors control demyelination and inflammation in the cuprizone model. Brain Behav Immun Health 4, 100062.
Bradley, J.E., Ramirez, G., Hagood, J.S., 2009. Roles and regulation of Thy-1, a context-dependent modulator of cell phenotype. Biofactors 35 (3), 258–265.
Caccavano, A., et al., 2020. Inhibitory parvalbumin basket cell activity is selectively reduced during hippocampal sharp wave ripples in a mouse model of familial Alzheimer's disease. J. Neurosci. 40 (26), 5116–5136.
Campagno, K.E., Mitchell, C.H., 2021. The P2X(7) receptor in microglial cells modulates the endolysosomal axis, autophagy, and phagocytosis. Front. Cell. Neurosci. 15, 645244.
Chen, Q., et al., 2012. Imaging neural activity using Thy1-GCaMP transgenic mice. Neuron 76 (2), 297–308.
Chu, T., et al., 2022. Cell type and gene expression deconvolution with BayesPrism enables Bayesian integrative analysis across bulk and single-cell RNA sequencing in oncology. Nat Cancer 3 (4), 505–517.
Conte, G., et al., 2020. High concordance between hippocampal transcriptome of the mouse intra-amygdala kainic acid model and human temporal lobe epilepsy. Epilepsia 61 (12), 2795–2810.
Conte, G., et al., 2020. P2X7 receptor-dependent microRNA expression profile in the brain following status epilepticus in mice. Front. Mol. Neurosci. 13, 127.
Dale, N., Frenguelli, B.G., 2009. Release of adenosine and ATP during ischemia and epilepsy. Curr. Neuropharmacol. 7 (3), 160–179.
Deuchars, S.A., et al., 2001. Neuronal P2X7 receptors are targeted to presynaptic terminals in the central and peripheral nervous systems. J. Neurosci. 21 (18), 7143–7152.
Di Virgilio, F., et al., 2017. The P2X7 receptor in infection and inflammation. Immunity 47 (1), 15–31.
Di Virgilio, F., Sarti, A.C., Coutinho-Silva, R., 2020. Purinergic signaling, DAMPs, and inflammation. Am. J. Physiol. Cell Physiol. 318 (5), C832–C835.
Diaz-Hernandez, M., et al., 2008. Inhibition of the ATP-gated P2X7 receptor promotes axonal growth and branching in cultured hippocampal neurons. J. Cell Sci. 121 (Pt 22), 3717–3728.
Dimidschstein, J., et al., 2016. A viral strategy for targeting and manipulating interneurons across vertebrate species. Nat. Neurosci. 19 (12), 1743–1749.
Dogan, E., et al., 2020. The role of NMDA receptors in the effect of purinergic P2X7 receptor on spontaneous seizure activity in WAG/Rij rats with genetic absence epilepsy. Front. Neurosci. 14, 414.
Dona, F., et al., 2009. Alteration of purinergic P2X4 and P2X7 receptor expression in rats with temporal-lobe epilepsy induced by pilocarpine. Epilepsy Res. 83 (2–3), 157–167.
Dravet, C., 2011. The core Dravet syndrome phenotype. Epilepsia 52 (Suppl 2), 3–9.
Dutton, S.B.B., et al., 2017. Early-life febrile seizures worsen adult phenotypes in Scn1a mutants. Exp. Neurol. 293, 159–171.
Engel, T., et al., 2012. Seizure suppression and neuroprotection by targeting the purinergic P2X7 receptor during status epilepticus in mice. FASEB J. 26 (4), 1616–1628.
Engel, T., et al., 2013. CHOP regulates the p53-MDM2 axis and is required for neuronal survival after seizures. Brain 136 (Pt 2), 577–592.
Engel, T., et al., 2018. Bi-directional genetic modulation of GSK-3beta exacerbates hippocampal neuropathology in experimental status epilepticus. Cell Death Dis. 9 (10), 969.
Engel, T., Smith, J., Alves, M., 2021. Targeting neuroinflammation via purinergic P2 receptors for disease modification in drug-refractory epilepsy. J. Inflamm. Res. 14, 3367–3392.
Fischer, W., et al., 2016. Critical Evaluation of P2X7 receptor antagonists in selected seizure models. PLoS One 11 (6), e0156468.
Garcia-Alonso, L., et al., 2019. Benchmark and integration of resources for the estimation of human transcription factor activities. Genome Res. 29 (8), 1363–1375.
Gilles, J.F., et al., 2017. DiAna, an ImageJ tool for object-based 3D co-localization and distance analysis. Methods 115, 55–64.
Gu, Z., Eils, R., Schlesner, M., 2016. Complex heatmaps reveal patterns and correlations in multidimensional genomic data. Bioinformatics 32 (18), 2847–2849.
Huang, C., et al., 2017. Inhibition of P2X7 receptor ameliorates nuclear factor-kappa B mediated neuroinflammation induced by status epilepticus in rat hippocampus. J. Mol. Neurosci. 63 (2), 173–184.
Illes, P., Khan, T.M., Rubini, P., 2017. Neuronal P2X7 receptors revisited: do they really exist? J. Neurosci. 37 (30), 7049–7062.
Jimenez-Mateos, E.M., et al., 2012. Silencing microRNA-134 produces neuroprotective and prolonged seizure-suppressive effects. Nat. Med. 18 (7), 1087–1094.
Jimenez-Mateos, E.M., et al., 2019. Regulation of P2X7 receptor expression and function in the brain. Brain Res. Bull. 151, 153–163.
Jimenez-Pacheco, A., et al., 2013. Increased neocortical expression of the P2X7 receptor after status epilepticus and anticonvulsant effect of P2X7 receptor antagonist A-438079. Epilepsia 54 (9), 1551–1561.
Jimenez-Pacheco, A., et al., 2016. Transient P2X7 receptor antagonism produces lasting reductions in spontaneous seizures and gliosis in experimental temporal lobe epilepsy. J. Neurosci. 36 (22), 5920–5932.
Kaczmarek-Hajek, K., et al., 2018. Re-evaluation of neuronal P2X7 expression using novel mouse models and a P2X7-specific nanobody. Elife 7.
Kim, J.E., Kang, T.C., 2011. The P2X7 receptor-pannexin-1 complex decreases muscarinic acetylcholine receptor-mediated seizure susceptibility in mice. J. Clin. Invest. 121 (5), 2037–2047.
Kim, Y.S., Yoon, B.E., 2017. Altered GABAergic signaling in brain disease at various stages of life. Exp Neurobiol 26 (3), 122–131.
Kinoshita, S., Koyama, R., 2021. Pro- and anti-epileptic roles of microglia. Neural Regen. Res. 16 (7), 1369–1371.
Kopp, R., et al., 2019. P2X7 interactions and signaling - Making head or tail of It. Front. Mol. Neurosci. 12, 183.
Leyh, J., et al., 2021. Classification of microglial morphological phenotypes using machine learning. Front. Cell. Neurosci. 15, 701673.
Liu, M., et al., 2020. Microglia depletion exacerbates acute seizures and hippocampal neuronal degeneration in mouse models of epilepsy. Am. J. Physiol. Cell Physiol. 319 (3), C605–C610.
Löscher, W., 2017. Animal models of seizures and epilepsy: past, present, and future role for the discovery of antiseizure drugs. Neurochem. Res. 42 (7), 1873–1888.
Love, M.I., Huber, W., Anders, S., 2014. Moderated estimation of fold change and dispersion for RNA-seq data with DESeq2. Genome Biol. 15 (12), 550.
Magloire, V., et al., 2019. GABAergic interneurons in seizures: Investigating causality with optogenetics. Neuroscientist 25 (4), 344–358.
Mamad, O., et al., 2023. Anti-seizure effects of JNJ-54175446 in the intra-amygdala kainic acid model of drug-resistant temporal lobe epilepsy in mice. Front. Pharmacol. 14, 1308478.
Maroso, M., et al., 2010. Toll-like receptor 4 and high-mobility group box-1 are involved in ictogenesis and can be targeted to reduce seizures. Nat. Med. 16 (4), 413–419.
Miller, A.R., et al., 2014. Mapping genetic modifiers of survival in a mouse model of Dravet syndrome. Genes Brain Behav. 13 (2), 163–172.
Miras-Portugal, M.T., et al., 2017. Neuronal P2X7 receptor: Involvement in neuronal physiology and pathology. J. Neurosci. 37 (30), 7063–7072.
Monif, M., et al., 2009. The P2X7 receptor drives microglial activation and proliferation: a trophic role for P2X7R pore. J. Neurosci. 29 (12), 3781–3791.

Morgan, J., et al., 2020. Characterization of the expression of the ATP-Gated P2X7 receptor following status epilepticus and during epilepsy using a P2X7-EGFP reporter mouse. Neurosci. Bull. 36 (11), 1242–1258.
Mouri, G., et al., 2008. Unilateral hippocampal CA3-predominant damage and short latency epileptogenesis after intra-amygdala microinjection of kainic acid in mice. Brain Res. 1213, 140–151.
Mula, M., 2011. GABAergic drugs in the treatment of epilepsy: modern or outmoded? Future Med. Chem. 3 (2), 177–182.
Nieoczym, D., Socala, K., Wlaz, P., 2017. Evaluation of the anticonvulsant effect of brilliant blue G, a selective P2X7 receptor antagonist, in the iv PTZ-, maximal electroshock-, and 6 Hz-induced seizure tests in mice. Neurochem. Res. 42 (11), 3114–3124.
Nosten-Bertrand, M., et al., 1996. Normal spatial learning despite regional inhibition of LTP in mice lacking Thy-1. Nature 379 (6568), 826–829.
Otrokocsi, L., Kittel, A., Sperlagh, B., 2017. P2X7 receptors drive spine synapse plasticity in the learned helplessness model of depression. Int. J. Neuropsychopharmacol. 20 (10), 813–822.
Papp, L., Vizi, E.S., Sperlagh, B., 2004. Lack of ATP-evoked GABA and glutamate release in the hippocampus of P2X7 receptor-/- mice. Neuroreport 15 (15), 2387–2391.
Pelegrin, P., 2021. P2X7 receptor and the NLRP3 inflammasome: Partners in crime. Biochem. Pharmacol. 187, 114385.
Pfisterer, U., et al., 2020. Identification of epilepsy-associated neuronal subtypes and gene expression underlying epileptogenesis. Nat. Commun. 11 (1), 5038.
Righes Marafiga, J., Vendramin Pasquetti, M., Calcagnotto, M.E., 2021. GABAergic interneurons in epilepsy: More than a simple change in inhibition. Epilepsy Behav. 121 (Pt B), 106935.
Rissiek, B., et al., 2015. P2X7 on mouse T cells: one channel, many functions. Front. Immunol. 6, 204.
Rozmer, K., et al., 2017. Pilocarpine-induced status epilepticus increases the sensitivity of P2X7 and P2Y1 receptors to nucleotides at neural progenitor cells of the juvenile rodent hippocampus. Cereb. Cortex 27 (7), 3568–3585.
Ruffolo, G., et al., 2022. GABA(A) receptor function is enhanced by Interleukin-10 in human epileptogenic gangliogliomas and its effect is counteracted by Interleukin-1beta. Sci. Rep. 12 (1), 17956.
Sahasrabuddhe, V., Ghosh, H.S., 2022. Cx3Cr1-Cre induction leads to microglial activation and IFN-1 signaling caused by DNA damage in early postnatal brain. Cell Rep. 38 (3), 110252.
Sloviter, R.S., et al., 2003. "Dormant basket cell" hypothesis revisited: relative vulnerabilities of dentate gyrus mossy cells and inhibitory interneurons after hippocampal status epilepticus in the rat. J Comp Neurol 459 (1), 44–76.
Smith, J., et al., 2023. The P2X7 receptor contributes to seizures and inflammation-driven long-lasting brain hyperexcitability following hypoxia in neonatal mice. Br. J. Pharmacol. 180 (13), 1710–1729.
Sperlagh, B., Illes, P., 2014. P2X7 receptor: an emerging target in central nervous system diseases. Trends Pharmacol. Sci. 35 (10), 537–547.
Surprenant, A., et al., 1996. The cytolytic P2Z receptor for extracellular ATP identified as a P2X receptor (P2X7). Science 272 (5262), 735–738.
Ta, H.M., et al., 2016. Atf6alpha deficiency suppresses microglial activation and ameliorates pathology of experimental autoimmune encephalomyelitis. J. Neurochem. 139 (6), 1124–1137.
Varvel, N.H., et al., 2016. Infiltrating monocytes promote brain inflammation and exacerbate neuronal damage after status epilepticus. PNAS 113 (38), E5665–E5674.
Vezzani, A., Balosso, S., Ravizza, T., 2019. Neuroinflammatory pathways as treatment targets and biomarkers in epilepsy. Nat. Rev. Neurol. 15 (8), 459–472.
Warnes, G., Bonebakker, L., Gentleman, R., Huber, W., Liaw, A., Lumley, T., Maechler, M., Magnusson, A., Moeller, S., Schwartz, M, Venables, B., 2022. gplots: Various R programming tools for plotting data.
Wickham, H., 2016. *ggplot2: Elegant graphics for data analysis*.
Wu, T., et al., 2021. clusterProfiler 4.0: A universal enrichment tool for interpreting omics data. Innovation (camb) 2 (3), 100141.
Yao, Z., et al., 2021. A taxonomy of transcriptomic cell types across the isocortex and hippocampal formation. Cell 184 (12), 3222–3241 e26.
Young, P., et al., 2008. Single-neuron labeling with inducible Cre-mediated knockout in transgenic mice. Nat. Neurosci. 11 (6), 721–728.
Yue, J., et al., 2022. Negative effects of brain regulatory T cells depletion on epilepsy. Prog. Neurobiol. 217, 102335.
Zhao, X.F., et al., 2019. Targeting microglia using Cx3cr1-Cre lines: revisiting the specificity. Eneuro 6 (4).